DEUTSCHES ELEKTRONEN – SYNCHROTRON

DESY 92-116
ENSLAPP-A-385/92
August 1992

Excited Fermions at e^+e^- and eP Colliders

F. Boudjema
Lab. de Phys. Théorique ENSLAPP, Annecy-le-Vieux, France

A. Djouadi
Deutsches Elektronen-Synchrotron DESY, Hamburg

J. L. Kneur
Fakultät für Physik, Universität Bielefeld

ISSN 0418-9833

NOTKESTRASSE 85 · D-2000 HAMBURG 52

To be sure that your preprints are promptly included in the
HIGH ENERGY PHYSICS INDEX,
send them to (if possible by air mail):

DESY
Bibliothek
Notkestraße 85
W-2000 Hamburg 52
Germany

DESY-IfH
Bibliothek
Platanenallee 6
O-1615 Zeuthen
Germany

ISSN 0418-9833

DESY 92-116
ENSLAPP-A-385/92

Excited Fermions at e^+e^- and eP Colliders

F. Boudjema[1], A. Djouadi[2] and J. L. Kneur[3]

[1] Laboratoire de Physique Théorique ENSLAPP*
Chemin de Bellevue, B.P. 110, F-74941 Annecy-le-Vieux, Cedex, France.

[2] Deutsches Elektronen–Synchrotron, DESY, D–2000 Hamburg 52, FRG.

[3] Fakultät für Physik, Universität Bielefeld, D-4800 Bielefeld, FRG.

ABSTRACT

We analyse the discovery potentials of future colliders with respect to excited fermions which are expected in models of fermionic substructure. After discussing the possibilities offered by LEP, we will consider in detail the Next Linear Collider in its e^+e^-, $e\gamma$ and $\gamma\gamma$ modes [where the high–energy photon beams are obtained through back–scattering of laser light]. In addition, since eP colliders are well adapted to the search of the first generation of excited leptons, we include a study of their possible manifestation at HERA and LEP/LHC. We give complete and compact formulae for decay widths, production cross sections and angular distributions. Furthermore, we analyse in some detail the polarisation of the produced excited fermions which allows for an easy reconstruction of the correlations between the initial state and the decay products of the heavy fermions.

*URA 14-36 du CNRS, associé à l'E.N.S de Lyon, et au L.A.P.P. d'Annecy-le-Vieux.

1 Introduction

The existence of excited states is the most unambiguous and characterizing signal for substructure in the fermionic sector [1, 2]. Indeed, if the known quarks and leptons are composite, they should be regarded as the ground state to a rich spectrum of excited states. The search for excited charged fermions has been systematically pursued for more than a quarter of a century now [3] but has not met with any success so far; while the search for excited neutrinos, which may be the lightest excited particles, have started in earnest only recently at LEP100 [4, 5]. For both types of particles, masses below 45 GeV have already been excluded [6]. Moreover, if the strength parametrizing their single production in Z decays is set at a scale of the order of 1 TeV, masses up to practically M_Z are also ruled out.

Though disappointing, this situation is not in conflict with the motivations behind the introduction of excited particles [1, 2]. Indeed, on the one hand, in analogy with systems of substructure spanning from molecular to atomic then hadronic classifications, one hopes to explain the well–ordered pattern of the fermionic spectrum with its three–fold replica by an as-yet new layer of matter whose scale describes the dynamics of the excited particles. On the other hand, compositeness is often invoked as a possible alternative to the conventional Standard Model description of electroweak symmetry breaking. It is then conceivable that the first excitations from the New Physics would only be felt at or above an energy scale intimately related to the Fermi scale which, within our present understanding, is the common scale behind the masses of all particles. Therefore, future colliders operating at such energies will play an important rôle, not only in unravelling the details of the still untested scalar sector but also in revealing a possible evidence for non–standard physics, such as the existence of excited fermions. Nonetheless, lacking an understanding of the origin of the Fermi scale and a predictive dynamical model of substructure one can not disregard the possibility that the excited states may appear below the Fermi scale already at LEP200 or HERA [or even at LEP100 if their couplings to the known particles are small hence requiring a higher luminosity to be collected].

In view of the phenomenological success of the Standard Model, one should generalize the "classic" electromagnetic interactions of the charged excited fermions [1] to include weak isodoublets of excited states [7–10]. The latter will then have full weak couplings to the gauge bosons. In addition, generalized magnetic–type couplings between the excited and ordinary states are present, allowing for the de–excitations of the excited fermions to the fundamental states consisting of the usual particles. These two types of couplings lead to the pair production of the excited fermions and their single production in association with the ordinary ones.

In the present paper, we perform a detailed analysis of the discovery potentials of future e^+e^- colliders for excited fermions. In addition to the upcoming LEP200 machine, we will discuss the case of the Next Linear e^+e^- Collider [NLC] that we assume to operate at a center of mass energy of 500 GeV [11, 12]. Besides the pair and single production of the excited states in the conventional e^+e^- annihilation mode, we will investigate the promising possibilities that are offered by the recently discussed $e\gamma$ and $\gamma\gamma$ colliders [13]. Indeed, the

single-pass future e^+e^- linear colliders can be turned into high-energy $e\gamma$ and $\gamma\gamma$ colliders through back-scattering of laser light on the initial electron/positron beams. These high-energy colliders, running with as much as 90% for $e\gamma$ and 80% for $\gamma\gamma$ of the original e^+e^- energy, open up the possibility of new production channels: pair and single production of excited charged fermions in $\gamma\gamma$ collisions and single production of excited electrons and neutrinos in $e\gamma$ collisions.

We will also investigate in some detail the possibilities offered by the eP colliders HERA and the planned LEP/LHC, which are well adapted to the search for the excited electron and its neutrino partner. The case of pp colliders, which are particularly efficient to probe excited quarks, has been studied in [14] and will not be considered here. In fact, for the sake of simplicity, we will only discuss in our numerical analysis the case of excited leptons, although it can readily be extended to include quarks as we give general formulae for any excited fermion.

We will give complete and compact formulae for the decay widths of the excited fermions, their production cross-sections and the angular distributions. Several [partial] analyses of the subject have been conducted in the past in the case of e^+e^- [7–10,15,16] and eP collisions [9, 17]. In this article, besides deriving new formulae for total cross-sections, we will extend the previous analyses by explicitely including the polarisation of the produced excited particles. Combined with the decays, this allows to fully take into account the correlation between the initial e^+e^- or eP states and the decay products of the final excited fermions. This approach lends itself to a straighforward adapatation into a fast Monte Carlo program. We have also given an equal importance to the search of excited neutrinos and considered the new decay channels of the excited charged leptons into the weak bosons. Earlier studies dealt mostly with excited charged leptons at low energies by considering their electromagnetic decays. A special emphasis on the extraction of the signal is given especially in the new environment of the NLC500 and LEP/LHC where the physics of weak bosons production is important. The single production of charged fermions at $\gamma\gamma$ has also been recently studied [18]. Our study is made so that a comparative analysis between the $e^+e^-$and $\gamma\gamma$ mode of the same collider may be conducted. Moreover, we give a particular attention to the competing backgrounds in $\gamma\gamma$ collisions and show how one can reduce them. In the case of $e\gamma$ collisions, we have reanalysed the by now classic e^* resonant production and we derived simple formulae for the whole process, production followed by decay either to $e\gamma$ or to νW. We point that the chiral structure of the Lagrangian allows to drastically reduce standard model backgrounds. Our analytical results for ν_e^* production in the $e\gamma$ mode are new.

The paper will be organized as follows. In the next section we first introduce the Lagrangian describing the interaction of the excited fermions. We will then discuss in detail the decay modes of the heavy fermions including the three body decays [which are very important for excited neutrinos with masses below M_W] and the spin-dependent differential widths of the heavy fermion. Having introduced the parameters of the excited fermions, we present the existing limits on the scale of compositeness and on the masses of the excited leptons in accord with our parametrization. In section 3, we study pair and single production of excited fermions in e^+e^- annihilation. In the case of pair production, possible effects of form factors [like for instance anomalous magnetic moments] will be taken into account. We

will also give the spin-dependent differential cross-section keeping both spins, so that the distributions between the final decay products may be investigated beside the correlation between the initial and final particles. For single production, we study angular distributions and polarisation effects, paying a special attention to the first generation of excited leptons for which additional production channels are present. After a discussion of the characteristics of the signals and the possible backgrounds, we derive discovery limits based on yearly integrated luminosities of 500 pb^{-1} at LEP200 and 10 fb^{-1} at the 500 GeV NLC. In section 4, we discuss the new possibilities provided by $e\gamma$ and $\gamma\gamma$ colliders. Besides the resonant production of excited electrons, which would be one of the best motivations for an $e\gamma$ collider, we will discuss the single production of excited electronic neutrinos in association with W bosons. The second part of section 4 is devoted to the pair production [where form factors will be included] and single production of charged excited fermions in $\gamma\gamma$ collisions. In section 5 we analyse the potential of the eP colliders HERA and LEP/LHC, with center of mass energies of 314 GeV and 1.26 TeV respectively, for the single production of excited leptons. To discriminate the produced excited leptons from other types of new leptons, we will show that the polarisation and the transverse momentum spectrum of the final heavy particles can be very useful. Finally, section 6 contains our conclusions. We draw a comparison of the expected discovery limits to be reached at the different colliders that we have considered. An Appendix is added which gives our conventions for the extraction of the degrees of longitudinal and transverse polarisation of the final excited fermion and sets the formalism for combining the spin-dependent decay distributions with the spin-dependent cross-sections to recover the full correlations between any particle from the decay of the excited heavy fermion.

2 Couplings, decay modes and present constraints

2.1 Couplings

In the present study, we will assume that the excited fermions have spin and isospin 1/2; higher spin and isospin assignments have been discussed in the literature [8] and will not be considered here. To accomodate the fact that the excited states are much heavier than the ordinary fermions, we will also assume that they acquire their masses prior to SU(2)×U(1) breaking. Hence, both their left–handed and right–handed components are in weak isodoublets. For instance, in the case of the first generation leptons, one has

$$l_L = \begin{bmatrix} \nu_e \\ e \end{bmatrix}_L \quad e_R \ ; \qquad L_L = \begin{bmatrix} \nu_e^* \\ e^* \end{bmatrix}_L \quad L_R = \begin{bmatrix} \nu_e^* \\ e^* \end{bmatrix}_R$$

and similarly for quarks and for the second and third families. The couplings of the excited fermions to the gauge fields are then vector–like. Denoting the excited fermion doublet by $F^* = F_L^* + F_R^*$, the interaction Lagrangian is given by[1]

$$\mathcal{L}_{f^*f^*} = \overline{F^*}\,\gamma^\mu \left[g\frac{\vec{\tau}}{2}\vec{W}_\mu + g'\frac{Y}{2}B_\mu + g_s\frac{\vec{\lambda}}{2}\vec{G}_\mu \right] F^* \qquad (2.1)$$

[1] In addition to these gauge interactions, contact interactions could arise from the interchange of the more elementary constituents [2]. The latter forces will not be considered here.

where $\vec{\tau}$ are the Pauli matrices, Y the weak hypercharge [$Y=-1$ for leptons and $Y=1/3$ for quarks] and g, g' the usual weak coupling constants $g = e_0/s_W$ and $g' = e_0/c_W$ [e_0 is the proton charge and $s_W^2 = 1 - c_W^2 \equiv \sin^2\theta_W \simeq 0.23$]; $\vec{\lambda}$ are the Gell-Mann matrices and g_s the strong coupling constant.

Due to the high masses of the excited particles and to their genuine composite nature, the vertices derived from the previous Lagrangian should be endowed with form factors and [possibly large] anomalous magnetic moments should be included. The most general couplings between a pair of excited fermions [with masses m_*] and a neutral boson V can then be written as

$$\Gamma_\mu^{Vf^*f^*} = ie_0\left[f_1^V\gamma_\mu + \frac{i}{2m_*}f_2^V\sigma_{\mu\nu}q^\nu + f_3^V\gamma_\mu\gamma_5 + \frac{i}{2m_*}f_4^V\sigma_{\mu\nu}\gamma_5 q^\nu\right] \tag{2.2}$$

where q is the four–momentum of the vector boson and m_* the mass of the excited fermion. In these couplings, f_1 refers to the charge form factor [with the q^2 part representing the charge radius], f_2 to the anomalous magnetic moment, the CP violating term f_4 represents the electric dipole moment for photons and f_3 parity violation [in fact, $U(1)_{em}$ gauge invariance does not allow such a coupling for photons, it should rather be replaced by $(q^2\gamma_\mu - q_\mu \not{q})\gamma_5/m_*^2$ which parametrizes an anapole form factor and vanishes for a real photon]. In addition, for the massive vector bosons, one can also have scalar and pseudo–scalar Vff couplings, q_μ and $q_\mu\gamma_5$, which in e^+e^- collisions give contributions which are proportional to the electron mass, and therefore are totally negligible. In the limit where the compositeness scale is very large, the form factors f_i reduce to the point-like couplings: the CP violating terms f_4 are absent, $f_2^V = 0$ at the tree level and in terms of the weak isospin and the electric charges

$$f_1^\gamma = v_f^\gamma = e_f \ , \qquad f_3^\gamma = a_f^\gamma = 0$$

$$f_1^Z = v_f^Z = \frac{2I_{3L}^f + 2I_{3R}^f - 4e_f s_W^2}{4s_W c_W} \ , \qquad f_3^Z = a_f^Z = \frac{2I_{3L}^f - 2I_{3R}^f}{4s_W c_W}$$

$$f_1^W = v_f^W = \frac{1}{2\sqrt{2}s_W} \ , \qquad f_3^W = a_f^W = \frac{1}{2\sqrt{2}s_W} \tag{2.3}$$

The Lagrangian describing the transition between excited fermions and ordinary fermions should respect a chiral symmetry in order to protect the light leptons from radiatively acquiring a large anomalous magnetic moment [19, 20]. This means that only the right-handed part of the excited fermions takes part in the generalized magnetic de–excitation. The latter is described in an $SU(2)\times U(1)$ invariant form by the following effective lagrangian [7–10]

$$\mathcal{L}_{ff^*} = \frac{1}{2\Lambda}\overline{F^*}\sigma^{\mu\nu}\left[gf\frac{\vec{\tau}}{2}\vec{W}_{\mu\nu} + g'f'\frac{Y}{2}B_{\mu\nu} + g_s f_s\frac{\vec{\lambda}}{2}\vec{G}_{\mu\nu}\right]f_L + \text{h.c} \tag{2.4}$$

Λ is to be understood as the scale of substructure while the constants f, f' and f_s are weight factors associated to the three gauge groups and can be interpreted as parametrizing different scales $\Lambda_i = \Lambda/f_i$ for the three groups. The tensors $V_{\mu\nu}$ represent the fully gauge–invariant

field tensors. The non–abelian part of the weak tensor $W_{\mu\nu}$ has interesting phenomenological consequences at high–energies since it gives rise to contact quartic (seagull) terms involving an excited fermion, an ordinary fermion and two gauge bosons: $e\nu^*W\gamma$, $e\nu^*WZ$, $\nu\nu^*W^+W^-$ and $ee^*W^+W^-$ and the self–conjugate vertices. Indeed, in the physical basis, the electroweak part of the Lagrangian eq. (2.4) can be written in terms of the components of the doublets (l, l') as follows

$$\mathcal{L}_{ff^*} = \frac{e}{2\Lambda}(f-f')N_{\mu\nu}\sum_{l=\nu,e}\bar{l}^*\sigma^{\mu\nu}l_L + \frac{e}{2\Lambda}f\sum_{l,l'=\nu,e}\Theta_{\mu\nu}^{\bar{l}^*,l}\ \bar{l}^*\sigma^{\mu\nu}l'_L + \text{h.c.} \tag{2.5}$$

where the first purely diagonal U(1) part, with $N_{\mu\nu} = \partial_\mu A_\nu - (s_W/c_W)\partial_\mu Z_\nu$, vanishes for $f = f'$; and the second non–abelian part involves the quartic terms

$$\begin{aligned}
\Theta_{\mu\nu}^{\bar{\nu}^*,\nu} &= \frac{1}{s_W c_W}\partial_\mu Z_\nu - i\frac{e}{s_W^2}W_\mu^+W_\nu^- \\
\Theta_{\mu\nu}^{\bar{e}^*,e} &= -\left(2\partial_\mu A_\nu + \frac{c_W^2 - s_W^2}{s_W c_W}\partial_\mu Z_\nu - i\frac{e}{s_W^2}W_\mu^+W_\nu^-\right) \\
\Theta_{\mu\nu}^{\bar{\nu}^*,e} &= \frac{\sqrt{2}}{s_W}\left(\partial_\mu W_\nu^+ - ieW_\mu^+(A_\nu + \frac{c_W}{s_W}Z_\nu)\right) \\
\Theta_{\mu\nu}^{\bar{e}^*,\nu} &= \frac{\sqrt{2}}{s_W}\left(\partial_\mu W_\nu^- + ieW_\mu^-(A_\nu + \frac{c_W}{s_W}Z_\nu)\right)
\end{aligned} \tag{2.6}$$

For the hermitian conjugate we only have to replace the left–handed lepton $l'_L = \frac{(1-\gamma_5)}{2}l'$ by the right handed anti–lepton $\bar{l}'_R = \bar{l}'\frac{(1+\gamma_5)}{2}$ while the operators Θ and N remain unchanged. These seagull terms are important since, for instance, the failure to include the $e\nu^*W\gamma$ term in the reaction $e\gamma \to W\nu^*$ does not give a gauge invariant amplitude.

Finally, the chiral couplings lead to the $V\bar{f}^*f$ vertex [V is a gauge boson with momentum q]

$$\Gamma_\mu^{Vf^*f} = \frac{e_0}{2\Lambda}q^\nu\sigma_{\mu\nu}(1-\gamma_5)f_V \tag{2.7}$$

where in terms of the weak isospin and the electric charges, f_γ, f_W and f_Z are

$$f_\gamma = e_f f' + I_{3L}(f-f') \ , \quad f_W = \frac{1}{\sqrt{2}s_W}f \ , \quad f_Z = \frac{4I_{3L}(c_W^2 f + s_W^2 f') - 4e_f s_W^2 f'}{4s_W c_W} \tag{2.8}$$

Unless otherwise stated, we will set f and f' to be equal which leads to

$$f_\gamma = e_f f \ , \quad f_W = \frac{1}{\sqrt{2}s_W}f \ , \quad f_Z = \frac{I_{3L} - e_f s_W^2}{s_W c_W}f \tag{2.9}$$

This not only reduces the number of parameters so that a more predictive analysis can be conducted, but is also more natural since for $f = f'$ the excited neutrino has no tree–level electromagnetic couplings [10]. Therefore, apart from the masses of the excited fermions, the only other parameter is the strength of the de–excitation coupling f/Λ.

2.2 Decay modes

Excited fermions will decay into light fermions plus [real or virtual] gauge bosons. If their masses are larger than M_Z, the main decay modes are two body decays. In the case where $f = f'$, the excited neutrino decays only into We and νZ while for the excited electron there is the additional photonic decay; see Fig. 1. The decay widths for $f^* \to Vf$ where $V = \gamma, Z$ or W are given by [M_V is the mass of the gauge boson]

$$\Gamma(f^* \to Vf) = \frac{\alpha}{4}\frac{m_*^3}{\Lambda^2} f_V^2 \left(1 - \frac{M_V^2}{m_*^2}\right)^2 \left(1 + \frac{M_V^2}{2m_*^2}\right) \tag{2.10}$$

For excited quarks, the additional decay $q^* \to qg$ accounts for more than 80% of the total decays. The width is given by eq. (2.10) with $\alpha \to 4\alpha_s/3$ and $f_V = f_s$.

The excited fermions have very narrow widths as shown in Tab. 1a/b for several mass values and for $\Lambda/f = \Lambda/f' = 1$ TeV. In the case of excited leptons with masses below 500 GeV, the total width is less than 1 GeV. Therefore, the mean decay paths of the excited fermions are always below sub–micron distances [even for $\Lambda/f \sim 10$ TeV], which means that if the excited particles are produced they would decay inside the detector without the possibility of experimentally resolving their decay vertex. With the one–parameter Lagrangian for the de–excitation coupling that we use, $f = f'$, the branching ratios are unambiguously predicted once the excited fermion mass is known. Moreover for masses much larger than M_W/M_Z, the branching ratios tend to asymptotic values as shown in Tab. 1a/b. From this table, one can see that the electromagnetic decay of the charged excited fermions is not the dominant one. For instance, in the case of the e^* it is just about 30%, compared to almost 100% for low masses. In the case of excited quarks, the electromagnetic decay, which would constitute the cleanest way for "tracking" these particles, is a very small fraction of all decays. Therefore, relying on this mode leads to a considerable loss of events. Nevertheless, it constitutes a very characteristic signature of excited fermions and could help to disentangle them from other exotic fermions, e.g. stemming from extended gauge models [21].

Note that one should not completely disregard the possibility that $f \neq f'$ which leads to interesting features especially for the excited neutrino [10]. Indeed this situation will lead to the decay $\nu^* \to \nu\gamma$ which, even when $f - f' \ll f$, would account for a sizeable fraction of all decays for $m_* < M_W$. Tab. 1c shows the $\nu^* \to \nu\gamma$ branching ratios for $f = 1.025, f' = 0.975$. As one can see, for a 50 GeV ν^* it represents 55% of all decays. This is due to the fact that this channel is a two–body decay and can be more important than the three–body decays, even for very small values of $f - f'$ [of course, it becomes negligible for ν^* masses larger than M_W, when the decay channel $\nu^* \to e^- W$ opens up]. This very distinctive decay mode is one of the most interesting at LEP100 and in fact, the excited neutrino has been looked for through this signature [4, 5]. It is worth pointing that even in a situation where $f = f'$ at the tree–level, this electromagnetic transition can be induced at the one–loop order. Another motivation for considering this mode is the observation that, if the excited states are genuinely composite being made of more fundamental charged constituents, then the electromagnetic coupling of the neutral bound–state may be sizeable, a situation akin to that of the neutron.

When produced, an excited fermion will have a certain degree of longitudinal and/or transverse polarisation depending on its production mode. It is, therefore, important to keep this information in the decay in order to have a correct description of the distribution and correlation of the observed decay products with the initial and possibly other final particles. Denoting the covariant spin–vector and the four–momentum of the heavy fermion by n_μ and p_μ respectively [with $n \cdot n = -1$ and $p \cdot n = 0$], the polarisation four–vector P_μ of the excited fermion is defined through the polarised differential decay width [in general with respect to some energy or angular variable, x]

$$\frac{\mathrm{d}\Gamma^{\mathrm{pol}}}{\mathrm{d}x} = \frac{1}{2}\frac{\mathrm{d}\Gamma^{\mathrm{unpol}}}{\mathrm{d}x} \times (1 + n \cdot P) \tag{2.11}$$

where Γ^{unpol} is the unpolarised decay. The transverse and longitudinal components of the polarisation vector are most conveniently expressed in the rest frame of the decaying particle with the longitudinal component along the flight direction in the laboratory frame $P_\mu = (0, P_\perp, 0, P_\parallel)$. More details are given in the Appendix.

In the process where the f^* decays into an ordinary fermion and a gauge boson which subsequently decays into two light fermions

$$f^*(p_1) \longrightarrow f(l_1)V(q) \longrightarrow f(l_1)\, f_1(p_2)\, \bar{f}_2(l_2) \tag{2.12}$$

the polarisation vector is given by

$$n.P = m_* \times \frac{\left[(v_f^V)^2 + (a_f^V)^2\right] P_S + 2 v_f^V a_f^V P_A}{\left[(v_f^V)^2 + (a_f^V)^2\right] U_S + 2 v_f^V a_f^V U_A} \tag{2.13}$$

where v_f^V/a_f^V are the vectorial/axial parts of the $f_1\bar{f}_2V$ couplings as given in eq. (2.3), and

$$\begin{aligned}
U_S &= 8(l_1 \cdot l_2)^2 + 4M_V^2(l_1 \cdot l_2) + m_*^2[m_*^2 - M_V^2 - 4(l_1 \cdot l_2)] \\
P_S &= 2(n \cdot p_2)[m_*^2 - 2(l_1 \cdot l_2) - M_V^2] + 4(n \cdot l_2)(l_1 \cdot l_2) \\
U_A &= m_*^2[m_*^2 - M_V^2 - 4(l_1 \cdot l_2)] \\
P_A &= 2(n \cdot p_2)[m_*^2 - 2(l_1 \cdot l_2) - M_V^2] - 4(n \cdot l_2)(l_1 \cdot l_2)
\end{aligned} \tag{2.14}$$

In the case where the V decay products are ignored, this expression becomes much simpler, since one has only to consider the two–body decay $f^*(p_1) \to f(l_1)V(q)$

$$n.P = m_* \times \frac{4(n \cdot q)(q \cdot l_1) - M_V^2\; n \cdot l_1}{4(p_1 \cdot q)(q \cdot l_1) - M_V^2\; p_1 \cdot l_1} \tag{2.15}$$

and for the electromagnetic decay $f^*(p_1) \to f(l_1)\gamma(q)$, a further simplification is obtained by setting $M_V^2 = 0$ in the previous expression

$$n.P = m_* \times (n \cdot q)/(q \cdot p_1) \tag{2.16}$$

For completeness, let us now discuss the decays of the excited fermions when their masses are smaller than the weak boson masses. This situation would still be compatible with the

experimental constraints if the compositeness scale Λ is significantly larger than 1 TeV. This leaves a window for future searches at a high-luminosity LEP100 [22].

The charged excited fermions still have the two-body decays $f^* \to f\gamma$ [unless $f = -f'$] and for quarks $q^* \to qg$. These decays account for practically the totality of the width. In the case of the excited neutrinos, the electromagnetic decay is not allowed if $f = f'$ and the ν^* can only have three body decays via an intermediate W or Z boson. In a previous publication [10] two of us derived the corresponding decay widths. For completeness, we will give here the analytic expressions of the partial widths in the general case where $f \neq f'$ and take the opportunity to correct two misprints which occured in the formulae given in [10].

The Feynman diagrams contributing to the decays are shown in Fig. 1. To simplify the formulae, we take advantage of the fact that $v_W = a_W$ and define the factor

$$G_{VV'} = \frac{\alpha^2}{8\pi} f_V f_{V'} \left(v_f^V v_f^{V'} + a_f^V a_f^{V'}\right) \frac{m_*^3}{\Lambda^2} N_c^f \tag{2.17}$$

In the case where the decay is mediated by W exchange $\nu^* \to Wl^- \to l^- f\bar{f}'$, using the reduced variables $w = M_W^2/m_*^2$ and $u = 2E_l/m_*$, the distribution $\mathrm{d}\Gamma_{WW}/\mathrm{d}u$ and the decay width Γ_{WW} are given by

$$\frac{\mathrm{d}\Gamma_{WW}}{\mathrm{d}u} = G_{WW}\left\{\frac{u[(1-2u)(1-2u+2w)+u]}{w-u} - [(1+2w)(1-u)+u(2u-2w-1)]\log\left(1-\frac{u}{w}\right)\right\}$$

$$\Gamma_{WW} = G_{WW}\left[\left(\frac{4}{3}w^3 - 2w + \frac{2}{3}\right)\log\left(1-\frac{1}{w}\right) + \frac{4}{3}w^2 + \frac{2}{3}w - \frac{14}{9}\right] \tag{2.18}$$

For the decay channel mediated by Z exchange, $\nu^* \to Z\nu \to \nu f\bar{f}$, using the variables $z = M_Z^2/m_*^2$ and $u = 2E_f/m_*$, one has for $\mathrm{d}\Gamma_{ZZ}/\mathrm{d}u$ and Γ_{ZZ}

$$\frac{\mathrm{d}\Gamma_{ZZ}}{\mathrm{d}u} = \frac{1}{3}G_{ZZ}\,\frac{u^2(1-u)(3-u)}{(1-u-z)^2}$$

$$\Gamma_{ZZ} = G_{ZZ}\left[\left(\frac{4}{3}z^3 - 2z + \frac{2}{3}\right)\log\left(1-\frac{1}{z}\right) + \frac{4}{3}z^2 + \frac{2}{3}z - \frac{14}{9}\right] \tag{2.19}$$

For the decay $\nu^* \to \nu l^+ l^-$ both Z and W exchange diagrams contribute and interference terms have to be taken into account. Defining again $u = 2E_l/m_*$, the decay distribution and the partial width are just the sum of the expressions given in eqs. (2.18, 2.19) and the following interference terms

$$\frac{\mathrm{d}\Gamma_{ZW}}{\mathrm{d}u} = 2G_{ZW}\left[u(u-2w) + 2w(u-w)\log(1-u/w)\right]\frac{1-u}{1-u-z} \tag{2.20}$$

$$\begin{aligned}\Gamma_{ZW} &= 2G_{ZW}\left\{z(1-z)(1-z-2w)\log\frac{z-1}{z} + w(1-w)(1-w-2z)\log\frac{w-1}{w} - 2zw\right.\\ &\times\ (z+w-1)\left[\log\left(1-\frac{1}{z}\right)\log\left(\frac{z+w-1}{w}\right) + \mathrm{Li}_2\left(\frac{z}{z+w-1}\right) - \mathrm{Li}_2\left(\frac{z-1}{z+w-1}\right)\right]\\ &+\ \left.\frac{5}{6} - \frac{7}{2}z + z^2 - 2w + 2zw\right\}\end{aligned}$$

where $\mathrm{Li}_2(x) = -\int_0^1 \mathrm{d}y\, y^{-1}\log(1-xy)$ is the usual Spence function.

The channel $\nu^* \to W^+ l^- \to l^- f\bar{f}'$ is always dominant [for instance, if $m_{\nu^*} = 45$ GeV, the branching ratio of the decay $\nu^* \to e^-$–jet–jet is $\simeq 50\%$] and for ν^* masses close to M_W it accounts for the totality of the width. For m_{ν^*} much smaller than M_W, the neutral channel has substantial contributions. The various branching ratios can be found in [10].

Finally, we note that one can also use the general formulae for the differential polarised decay widths eqs. (2.13, 2.14), with the replacement $M_V^2 = q^2$ where q^2 represents the invariant mass of the $f_1\bar{f}_2$ system. This may be helpful to use by experimentalists to account for all possible distributions [with initial state correlations] including experimental cuts and taking into account particular detector geometries.

2.3 Present constraints

Before closing this section, let us briefly discuss the available constraints on the masses of the excited leptons and on the transition factor f/Λ. The most stringent and unambiguous limits on the excited leptons masses come from LEP100 data. From the negative search of these new states and from the measurement of Z decay widths at LEP, one obtains [6] assuming purely vectorial couplings: $m_{\nu^*} \geq 45.4$ GeV [independently of the transition factor f/Λ and the decay topologies of the ν^*] and $m_{e^*} \geq 45$ GeV [assuming that the e^* photonic decay is dominant]. For masses larger than $M_Z/2$, one can obtain bounds on the factor Λ/f for a given m_* value. For instance, in the case of charged leptons with masses of 50 GeV, Λ/f values larger than ~ 2 TeV have been excluded assuming $f' = f$ [the exact numbers are 2.24 TeV for e^* and μ^* and 1.6 TeV for τ^*]; see Table 2. Much weaker values for this factor are obtained for l^* masses close to the Z mass. For excited neutrinos, the limits critically depend on the chosen f and f' values. For ν^* masses of 50 GeV, a limit $\Lambda/f > 3.2$ TeV [for $m_{\nu^*} = 75$ GeV, $\Lambda/f > 2.3$ TeV] has been set by the ALEPH collaboration [4] which only looked at the radiative photonic decay, hence implicitely assuming $f = -f'$. The L3 collaboration [5] has also considered the decay $\nu_e^* \to eW$ and the results translate into the bound $\Lambda/f > 1$ TeV for $m_{\nu^*} = 50$ GeV and $f = -f'$. In the case of the e^*, complementary bounds on Λ/f have been extracted by looking at possible deviations from the predicted QED angular distribution of the process $e^+e^- \to \gamma\gamma$ due to e^* t-channel exchange. However, the LEP data give only a bound of $\Lambda/f > 100$ GeV [23] slightly stronger than the one obtained by the CELLO collaboration [24].

Indirect limits on the transition factor f/Λ come essentially from considering the contribution of the excited fermions to the anomalous magnetic moments of the electron and muon. Unfortunately, none of the calculations that we are aware of have been made for the case of a weak isodoublet structure with a full $SU(2) \times U(1)$ gauge invariant form. For instance, in the extensive investigation of the effects of excited fermions performed by Méry et al. [25], although ν^* contributions are taken into account, the contact term $\nu^* eW\gamma$ which contributes at the same order is missing. In an ealier paper, Renard [20] had considered only the purely electromagnetic de–excitation Lagrangian. Therefore, the present bounds $\Lambda/f > 800$ GeV [20, 25] coming from the $(g-2)_\mu$ can only serve as an order of magnitude estimate.

3 Production in e^+e^- Collisions

3.1 Pair Production

In e^+e^- collisions, excited fermions can be pair produced through s–channel gauge boson exchange Fig. 2a, if their masses are smaller than the beam energy. For charged fermions the process proceeds through γ, Z exchange while only Z exchange is present for excited neutrinos. For the first family of excited leptons, pair production is also possible through t–channel exchanges: W exchange for the ν_e^* and Z, γ exchanges for the e^*. These contributions represent a double de–excitation and can be safely neglected since the effective transition coupling is at most $fE_{\rm beam}/\Lambda$ and thus much smaller than the corresponding standard coupling which enters in the production through s–channel exchange[2]. In any case, if these t–channel contributions were of any significance for the double production mechanism then, *a fortiori*, the excited fermions are much more copiously produced singly; Fig. 2b.

If the excited fermions have the standard vectorial couplings, as described by the Lagrangian given in eq. (2.1), all flavours are produced with the same angular distribution

$$\frac{1}{\sigma}\frac{{\rm d}\sigma}{{\rm d}\cos\theta} = \frac{3}{4}\,\frac{(1-\beta^2)+(1+\beta^2\cos^2\theta)}{3-\beta^2} \tag{3.1}$$

where $\beta = (1-4m_*^2/s)^{1/2}$ is the velocity of the final excited fermion and θ specifies its direction with respect to the initial electron beam. Because of the vectorial nature of the f^* couplings, there is no forward–backward asymmetry contrary to the production of sequential charged and neutral fermions. Due to the excited fermion mass dependence, the distribution is also distinctive from that of a heavy Majorana neutrino pair, for which it can be shown, on very general grounds [26], that the angular distribution is proportional to $1+\cos^2\theta$. Of course, for light excited fermions the distribution tends to the one describing a Majorana pair. If the production of a pair of excited fermions is confirmed through their distinctive decay pattern [see below] and once their mass has been extracted, the $\cos\theta$ dependence is unambiguously given, independently of the strength of the vectorial couplings.

The presence of possibly large magnetic moments and form factors, which would be naturally associated with particles reflecting substructure, significantly distorts this distribution. We have allowed for such moments by considering the more general Lagrangian including electromagnetic and Z form factors as given in eq. (2.2). The resulting differential cross section can be conveniently written as [the summation over repeated indices as well as the complex conjugation of one of the couplings are understood]

$$\frac{{\rm d}\sigma}{{\rm d}\cos\theta} = \sigma_0 N_c \frac{3}{4}\beta\left\{(v_\alpha v_\beta + a_\alpha a_\beta)\left[A_1^{\alpha\beta} + A_2^{\alpha\beta}\cos^2\theta\right] + (v_\alpha a_\beta + a_\alpha v_\beta)A_3^{\alpha\beta}\cos\theta\right\} \tag{3.2}$$

[2]Note that in general, t–channel production mechanisms in e^+e^- collisions are crucially dependent on the chiral structure at the e^+ or e^- vertex so that one can check for their presence by polarising the initial beams. In our case, polarising the electron to be right–handed switches off this contribution. Of course, to allow for the s–channel contributions to proceed, one has either to use an unpolarised positron beam or a left-handed polarised positron.

where N_c is a colour factor, σ_0 the point like QED cross section, $\sigma_0 = 4\pi\alpha^2/3s$, and

$$\alpha,\beta = \gamma, Z \;\;,\qquad v^\gamma(a^\gamma) = v_e^\gamma(a_e^\gamma) \;\;,\qquad v^Z(a^Z) = v_e^Z(a_e^Z)\frac{s}{s-M_Z^2+i\Gamma_Z M_Z} \tag{3.3}$$

$$\begin{aligned}
A_1^{\alpha\beta} &= f_1^\alpha f_1^\beta - \frac{\beta^2}{2}(f_1^\alpha f_1^\beta - f_3^\alpha f_3^\beta) + f_1^\alpha f_2^\beta + f_2^\alpha f_1^\beta + \frac{1}{2}\left(\frac{s}{4m_f^2}+1\right)f_2^\alpha f_2^\beta + \frac{1}{2}\left(\frac{s}{4m_f^2}-1\right)f_4^\alpha f_4^\beta \\
A_2^{\alpha\beta} &= \frac{\beta^2}{2}\left[f_1^\alpha f_1^\beta + f_3^\alpha f_3^\beta - \frac{s}{4m_f^2}f_2^\alpha f_2^\beta - \frac{s}{4m_f^2}f_4^\alpha f_4^\beta\right] \\
A_3^{\alpha\beta} &= \beta\left[f_1^\alpha f_3^\beta + f_3^\alpha f_1^\beta + f_1^\alpha f_2^\beta + f_2^\alpha f_1^\beta\right]
\end{aligned} \tag{3.4}$$

In the point like–limit, the coefficients $A_{1,2,3}^{\alpha\beta}$ reduce to the usual form

$$A_1^{\alpha\beta} = \frac{2-\beta^2}{2}v_f^\alpha v_f^\beta + \frac{\beta^2}{2}a_f^\alpha a_f^\beta \;,\;\; A_2^{\alpha\beta} = \frac{\beta^2}{2}(v_f^\alpha v_f^\beta + a_f^\alpha a_f^\beta) \;,\;\; A_3^{\alpha\beta} = \beta(v_f^\alpha a_f^\beta + a_f^\alpha v_f^\beta) \tag{3.5}$$

From the differential cross section, eq. (3.2), one readily obtains the total cross section σ, the forward–backward asymmetry A_{FB} and the parameter κ_θ defined by ${\rm d}\sigma/{\rm d}\cos\theta \propto 1+\kappa_\theta\cos^2\theta$. Expressed in terms of the form factors, one has

$$\begin{aligned}
\sigma &= \frac{3}{2}N_c\sigma_0\beta_f(v_\alpha v_\beta + a_\alpha a_\beta)\left(A_1^{\alpha\beta} + \frac{1}{3}A_2^{\alpha\beta}\right) \\
A_{FB} &= \frac{1}{2}\frac{(v_\alpha a_\beta + a_\alpha v_\beta)A_3^{\alpha\beta}}{(v_\alpha v_\beta + a_\alpha a_\beta)\left(A_1^{\alpha\beta} + \frac{1}{3}A_2^{\alpha\beta}\right)} \\
\kappa_\theta &= \frac{(v_\alpha v_\beta + a_\alpha a_\beta)A_2^{\alpha\beta}}{(v_\alpha v_\beta + a_\alpha a_\beta)A_1^{\alpha\beta}}
\end{aligned} \tag{3.6}$$

In the case where the form factors and anomalous magnetic moments are neglected, the total cross section simplifies to [we drop the subscript Z in the $\bar{f}fZ$ couplings]

$$\sigma = \sigma_0 N_c \frac{(3-\beta^2)}{2}\beta\left[e_e^2 e_f^2 + \frac{2e_e v_e e_f v_f}{1-M_Z^2/s} + \frac{(a_e^2+v_e^2)v_f^2}{(1-M_Z^2/s)^2}\right] \tag{3.7}$$

The total cross sections for excited lepton pair production are shown in Fig. 3 for two center of mass energies: $\sqrt{s} = 200$ GeV typical of LEP200 and $\sqrt{s} = 500$ GeV as expected in a "first stage" e^+e^- linear collider. The cross sections are displayed in the case where the couplings of the excited leptons to gauge bosons are point–like, and in the presence of form factors: $f_1 = v_f^V(1+s/\Lambda^2)$ and $f_2 = m_*^2/\Lambda^2$ with $\Lambda = 1$ TeV. As can be seen from the figure, this special choice for the form factors enhances the cross sections: slightly at LEP200 but more importantly at the NLC, due to the energy and m_* dependence of the form factors.

To study the event rates and the signatures we restrict our discussion to the canonical case of purely vectorial couplings without form factors.

At LEP200, the production cross section for excited charged leptons of masses up to 70 GeV, is of the order of 3 pb and depends only slightly on m_{l^*}. For such masses, the branching ratio of the l^* decay into a photon and an ordinary charged lepton is $\simeq 100\%$. With the expected integrated luminosity of 500 pb^{-1}, one collects about 1500 events consisting of two very hard photons and a well separated acoplanar lepton–antilepton pair. These are very clean and background–free signals. Even for an excited charged lepton with a mass of 98 GeV, the signal is still prominent with about 500 events. The decay of both l^* into W and neutrinos seems to be difficult to exploit just above the $e^+e^- \to W^+W^-$ threshold, especially since in this mass range the branching ratio is below 30%.

For excited neutrino production, the cross section is smaller than for their charged partners due to the absence of the photon channel: for $m_{\nu^*} < 70$ GeV it is of the order of 2 pb. For such masses, one can use the three–body decays of both excited neutrinos into charged leptons plus jet–pairs, which result in about 600 events. Since both heavy neutrinos get a large enough boost, there will be two well separated systems of lepton–jets in one hemisphere, and an antilepton with the same flavour plus jets in the opposite hemisphere. For masses above M_W, the decay of both neutrinos into real W's and the corresponding ordinary leptons is a clean signal as it results in a W^+W^- pair and two prompt isolated leptons, with opposite charges but of the same species, and without missing energy.

At the NLC with a center of mass energy $\sqrt{s} = 500$ GeV, the rate for charged excited lepton production is $\simeq 500$ fb for masses around 150 GeV. For such masses, the branching ratio for the electromagnetic decay is only $\sim 30\%$ but the signature can still be used since, assuming an integrated luminosity of 10 fb^{-1}, one has about 500 events. In the case of excited neutrinos, for which the cross section is about three times smaller because of the absence of the dominant photon exchange, a clear signature would be the one where a ν^* goes into a light neutrino and a Z boson, which then decays invisibly, while the other ν^* decays via a W which subsequently decays into hadrons. We would then have a topology with one empty hemisphere with a large missing energy [totalling the beam energy] and a large missing transverse momentum, while the other hemisphere would contain an isolated energetic lepton and jets with an invariant mass equal to M_W. Although this signal would account for only 3% of all the events, one collects about 35 events for $m_{\nu^*} = 150$ GeV with a luminosity of 10 fb^{-1}.

Therefore it is clear that excited leptons with their very spectacular signatures can be observed for masses up to the beam energy.

We have also analysed the degree of longitudinal and transverse polarisation of one of the excited fermions which may be introduced through

$$\left.\frac{\mathrm{d}\sigma}{\mathrm{d}\cos\theta}\right|^{\mathrm{pol}} = \left.\frac{\mathrm{d}\sigma}{\mathrm{d}\cos\theta}\right|^{\mathrm{unpol}} \times\ (1 + P\cdot n) \tag{3.8}$$

where n is the spin vector of the particle. In the case where anomalous magnetic moments and form factors are absent, the longitudinal $P_{\|}$ and transverse $P_\perp$ components of the polarisation vector $P = (0, P_\perp, 0, P_{\|})$ of the f^* in its rest frame are given by

$$\begin{aligned} P_{\|} &= -\ \frac{2(v_\alpha a_\beta + a_\alpha v_\beta)\left[A_1^{\alpha\beta} + A_2^{\alpha\beta}\right]\cos\theta + (v_\alpha v_\beta + a_\alpha a_\beta)A_3^{\alpha\beta}(1+\cos^2\theta)}{(v_\alpha v_\beta + a_\alpha a_\beta)\left[A_1^{\alpha\beta} + A_2^{\alpha\beta}\cos^2\theta\right] + (v_\alpha a_\beta + a_\alpha v_\beta)A_3^{\alpha\beta}\cos\theta} \\ P_\perp &= \frac{2m_{l^*}}{\sqrt{s}}\sin\theta\,\frac{(v_\alpha v_\beta + a_\alpha a_\beta)A_3^{\alpha\beta}\cos\theta + 2(v_\alpha a_\beta + a_\alpha v_\beta)v_f^\alpha v_f^\beta}{(v_\alpha v_\beta + a_\alpha a_\beta)\left[A_1^{\alpha\beta} + A_2^{\alpha\beta}\cos^2\theta\right] + (v_\alpha a_\beta + a_\alpha v_\beta)A_3^{\alpha\beta}\cos\theta} \end{aligned} \tag{3.9}$$

where the coefficients $A_{1,2,3}^{\alpha,\beta}$ are given in eq. (3.5). Note that the polarisation vector has also a component which is normal to the production plane [27] but it is very small since it is generated by the imaginary part of the γ, Z interference, and therefore is proportional to the width of the Z boson [see the Appendix for more details on the polarisation]. The longitudinal and transverse components of the polarisation vectors of e^* and ν^* are shown in Fig. 4 as a function of the scattering angle, for $\sqrt{s} = 500$ GeV and $m_{l^*} = 150$ GeV. The magnitude of $P_{\|}$ and $P_\perp$ is approximately four times larger for the e^* than for the ν^* but the shape is exactly the same. $P_\perp$ is positive, forward–backward symmetric and maximal (minimal) for $\cos\theta = \pm 1\,(0)$. $P_{\|}$ is monotonically decreasing for increasing $\cos\theta$ and is zero for $\cos\theta = 0$. Averaging over the polar angle, one obtains the total transverse and longitudinal polarisations of the produced fermion. In the case where only purely vectorial couplings are assumed, there is no net longitudinal polarisation while the transverse polarisation is small

$$< P_{\|} > = 0\ , \qquad < P_\perp > = \frac{3\pi}{2}\frac{m_{l^*}}{\sqrt{s}}\frac{1}{3-\beta^2}\frac{(v_\alpha a_\beta + a_\alpha v_\beta)v_f^\alpha v_f^\beta}{(v_\alpha v_\beta + a_\alpha a_\beta)v_f^\alpha v_f^\beta} \tag{3.10}$$

We have also obtained the correlation between the decay products of the two final excited leptons by simultaneously keeping the spin dependence of both the heavy fermions. Again considering the case of canonical couplings, the differential cross section for the process $e^+(l_2)\ e^-(l_1) \to \bar{f}^*(p_2, n_2)\ f^*(p_1, n_1)$ writes

$$\begin{aligned} \frac{\mathrm{d}\sigma}{\mathrm{d}\cos\theta} = \frac{3}{8}\sigma_0 N_c \beta \Big\{ &\left[(2-\beta^2\sin^2\theta) + n_1^\mu n_2^\nu\left(\beta^2\sin^2\theta\ g_{\mu\nu} - \frac{4}{s}\left(L^+_{\mu\nu} + \beta\cos\theta\ L^-_{\mu\nu}\right)\right)\right] Q_1 \\ &+ \left[4\frac{m_{l^*}}{s}(n_1+n_2)\cdot(l_1-l_2)\right] Q_2 \Big\} \end{aligned} \tag{3.11}$$

with the generalized charges Q_1 and Q_2 given by

$$\begin{aligned} Q_1 &= e_f^2 e_e^2 + \frac{2e_e e_f v_e v_f}{1 - M_Z^2/s} + \frac{(v_e^2 + a_e^2)v_f^2}{(1 - M_Z^2/s)^2} \\ Q_2 &= \frac{2e_e a_e e_f v_f}{1 - M_Z^2/s} + \frac{2a_e v_e v_f^2}{(1 - M_Z^2/s)^2} \end{aligned} \tag{3.12}$$

and the tensors $L^\pm_{\mu\nu}$

$$\begin{aligned} L^-_{\mu\nu} &= l_{1\mu}l_{2\nu} - l_{1\nu}l_{2\mu} \\ L^+_{\mu\nu} &= l_{1\mu}l_{2\nu} + l_{1\nu}l_{2\mu} + 2(l_1+l_2)_\mu(l_1+l_2)_\nu \end{aligned} \tag{3.13}$$

These expressions should be combined with the polarised decays, as explained in the Appendix, to derive any distribution in terms of the final products variables.

3.2 Single Production

In e^+e^- annihilation, excited fermions can also be produced singly in association with their ordinary partners; Fig. 2b. Therefore, in principle, masses up to the total energy of the collider may be probed. The production rates depend on the parameter f/Λ in the de–excitation Lagrangian which measures the strength of the transition. The production proceeds through s–channel γ and Z exchange for all excited charged fermions, while for neutrinos only s–channel Z exchange is present for the choice $f = f'$. For the first generation of excited leptons, one has additional t–channel contributions: W exchange in the case of the excited electronic neutrino and Z boson and the all important γ exchange in the case of the excited electron. These t–channel contributions are very important as soon as one moves to energies away from the Z peak[3]. These processes should be compared to the single production of exotic heavy fermions predicted by extended gauge models [21]. However, in the latter case, there is no photon exchange and the couplings are not of the magnetic type.

In order to fully take into account the angular correlations of the decay products of the excited fermions, we calculated the complete differential cross section including the spin dependence of the heavy fermion. Combined with the formulae for the decay products presented in the previous paragraph, this allows for a straightforward Monte-Carlo implementation. We have checked that the non–spin dependent terms agree with a previous calculation [9]. With θ being the angle between the electron and the excited state f^*, the spin–dependent differential cross section for the process $e^+e^- \to \bar{f}f^*$ writes

$$\frac{\mathrm{d}\sigma}{\mathrm{d}\cos\theta}\,[e^+(l_2)e^-(l_1) \longrightarrow \bar{f}(p_2)f^*(p_1,n)] \;=\; N_c\sigma_0\frac{3}{16}\frac{s}{\Lambda^2}\beta\sum_{i=1}^{6}A_i^f R_i \qquad (3.14)$$

where in terms of $\beta = 1 - m_*^2/s$ and the fermion momenta, the expressions of R_i are

$$\begin{aligned}
R_1 &= 2\beta(1-\beta) + \beta^2(1-\cos^2\theta) + 2\frac{m_*}{s}\beta[n\cdot l_1(1+\cos\theta) + n\cdot l_2(1-\cos\theta)]\\
R_2 &= 2\beta(1-\beta)\cos\theta + 2\frac{m_*}{s}\beta[n\cdot l_1(1+\cos\theta) - n\cdot l_2(1-\cos\theta)]\\
R_3 &= \frac{1}{2}\beta^2(1-\cos^2\theta) + \frac{1}{2}\frac{m_*}{s}\beta(1+\cos\theta)[2n\cdot p_2 + n\cdot l_1\beta(1-\cos\theta) - n\cdot l_2\beta(1+\cos\theta)]\\
R_4 &= \frac{\beta}{2}(1-\cos\theta)[\cos\theta\beta(1+\beta) + \beta^2 - \beta + 2] + \frac{m_*}{s}\beta(1-\cos\theta)[n\cdot p_2\beta(1+\cos\theta) + 2n\cdot l_2]\\
R_5 &= -\frac{1}{2}\beta(1-\cos\theta)(1-\beta)(\beta\cos\theta + \beta + 2) + \frac{m_*}{s}\beta(1-\cos\theta)[n\cdot p_2\beta(1+\cos\theta) - 2n\cdot l_2]\\
R_6 &= -4\frac{m_e^2}{s}(1-\beta)^2 - 4\frac{m_*}{s}\frac{m_e^2}{s}(1-\beta)[2n\cdot l_2 - 2n\cdot p_2] \qquad (3.15)
\end{aligned}$$

Using the rescaled variables $z = M_Z^2/s, w = M_W^2/s$ and $r \equiv t/s = -\frac{1}{2}\beta(1-\cos\theta)$, the coefficients A_i^f are given by [we drop the indices Z in a_e^Z and v_e^Z]

$$A_1^f = e_e^2 f_\gamma^2 + \frac{2e_e v_e f_\gamma f_Z}{1-z} + \frac{(a_e^2+v_e^2)f_Z^2}{(1-z)^2}\;, \quad A_2^f = \frac{2e_e a_e f_\gamma f_Z}{1-z} + \frac{2a_e v_e f_Z^2}{(1-z)^2}$$

$$A_3^\nu = \frac{4v_W f_W}{r-w}\left[e_e f_\gamma + \frac{(a_e+v_e)f_Z}{1-z}\right]\;, \quad A_4^\nu = A_5^\nu = \frac{2v_W^2 f_W^2}{(r-w)^2}\;, \quad A_6^\nu = 0$$

$$A_3^e = 2\left[\frac{e_e^2 f_\gamma^2}{r} + e_e(a_e+v_e)\left(\frac{f_\gamma f_Z}{r(1-z)} + \frac{f_\gamma f_Z}{r-z}\right) + \frac{(a_e+v_e)^2 f_Z^2}{(1-z)(r-z)}\right]\;, \quad A_6^e = \frac{e_e^2 f_\gamma^2}{r^2}$$

$$A_4^e = \frac{e_e^2 f_\gamma^2}{r^2} + \frac{2e_e v_e f_\gamma f_Z}{r(r-z)} + \frac{(a_e^2+v_e^2)f_Z^2}{(r-z)^2}\;, \quad A_5^e = \frac{2e_e a_e f_\gamma f_Z}{r(r-z)} + \frac{2a_e v_e f_Z^2}{(r-z)^2} \qquad (3.16)$$

These formulae can also be used for excited fermions searches around the Z peak at LEP100. In this case, only the s–channel Z boson parts R_1 and R_2 should be kept [the latter contribution being very small because of the smallness of the vectorial coupling of the electron to the Z, v_e] and the finite width of the Z boson has to be introduced in the propagator.

[3]Note that, in view of the specific chiral structure of the de–excitation Lagrangian, these contributions are very sensitive to the longitudinal polarisation of the initial beams. For instance, a right-handed electron forbids the t–channel formation of both ν_e^* and $\overline{\nu_e^*}$ and reduces considerably the event rate for e^{*-} production relative to e^{*+}, by switching–off the photon and Z boson exchanges. Note also that with the polarisation of the initial beams, one can also considerably reduce one of the main background reactions: W pair production.

a) Angular distributions and polarisation

In Fig. 5, we show the angular distributions for the single production of e^*, ν_e^*, μ^* and ν_μ^* [where μ generically stands also for τ]. We have fixed the excited lepton masses to 150 GeV at LEP200 and 300 GeV at the 500 GeV NLC. These distributions help to compare the relative importance of the different s and t–channel contributions.

At both LEP200 and NLC energies, the angular distribution of the ν_μ^* where only the s–channel Z exchange is present, is rather flat. The angular distribution of μ^* production which proceeds via s–channel γ, Z exchange slightly favours the forward direction. For both fermions, the forward–backward asymmetries are due to the interference between their couplings and the axial coupling of the initial electron to the Z. Because of the smallness of v_e, the asymmetry is much less important for the excited neutrinos than for the charged leptons for which there is an additional contribution from Z–γ interference. The angular distribution for the production of excited electrons displays a dramatic forward peak due to the t–channel photon exchange.

In the case of the ν_e^* the angular distribution crucially depends on the center of mass energy: the forward peak due to the t–channel W exchange is dramatic at the NLC while at LEP200 it is modest. However, in the exact forward direction, the latter contribution vanishes and there, only remains the s–channel Z exchange contribution so that the cross section is at exactly the same level as that for the ν_μ^*. The t–channel contribution also vanishes in the exact backward direction and there again, the excited neutrinos of any flavour [and with the same masses] are produced with the same rate. This can be explicitely seen by looking at the contributions of the pure W exchange R_4 and R_5 terms which are proportional to

$$\frac{1-\cos^2\theta}{[1-\cos\theta + 2M_W^2/(s-m_*^2)]^2}\left[1 + \frac{2m_*}{s\beta}\,n.p_2\right] \qquad (3.17)$$

the contribution of the interference between the s and t–channel exchanges [R_3 term] being also proportional to $(1-\cos^2\theta)$. This feature is a reflection of the specific chiral structure of the de–excitation couplings: in the W t–channel contribution, the standard V–A interaction restricts the incoming positron to be right–handed [the antineutrino is also right–handed] while at the same time, the de–excitation vertex restricts the incoming electron to be left-handed. Therefore, the total angular momentum along the beam direction is equal to -1 i.e. is opposite to the e^- direction. In the backward scattering the spin of the ordinary right–handed antineutrino is necessarily $+1/2$ [pointing opposite to the e^- direction] and therefore, angular momentum conservation forbids this configuration. Note, that for the backward scattering we did not have to appeal to the polarisation state of the ν_e^*. Consider now the case of the forward scattering. The ordinary antineutrino has its spin along those of the e^+ and e^-, but the magnetic–type de–excitation flips the spin so that the excited neutrino necessarily has its spin pointing in the opposite direction to all the other spins. Again, angular momentum is in conflict with chirality and no forward scattering occurs[4].

One can pursue this line of thought for the other channels to get more physical insight. In the high–energy limit where all fermion masses may be neglected, the notions of chirality and helicity states are interchangeable. In this case, the right–handed excited fermion and the right–handed ordinary final antilepton both have helicity $+1/2$ while the electron and positron have opposite helicities. Therefore, if one projects the helicity amplitudes on the partial waves [in fact only the $J=1$ is possible] the only functions which appear are the $d^1_{\pm 1,0}$ functions which are proportional to $\sin\theta$. This can be more directly seen by taking the limit $\beta=1$ in the expressions of R_1–R_5 in eq. (3.15). Hence, in the chiral limit, there is no forward or backward scattering. Of course, this argument cannot apply in the case of excited electrons production in the very forward direction because of the t–channel photon exchange, since one cannot take the chiral limit for the electron/positron whose masses are needed to regulate the cross section at zero–momentum transfer. This gives a very strong forward peak at all energies. For ν_e^*, neglecting the small interference between s and t–channel contributions, the forward peak occurs at $\cos\theta \simeq 1/(1+2w/\beta)$ [$\simeq 0.92$ at NLC for $m_* = 300$ GeV]. This shows again that the peaking is more pronounced for lighter particles or higher energies.

Let us now briefly comment on the degree of longitudinal and transverse polarisations of the produced excited fermion, which are shown in Fig. 6a for LEP200 and Fig. 6b for the NLC. For the excited electronic neutrino, the behaviour can be understood by the dominance of the W exchange especially at higher energies as discussed above: at the 500 GeV NLC, a 300 GeV excited neutrino is longitudinally polarised for almost all production angles. For the excited electron, this state of polarisation is reached only in the very forward direction, but since this region accounts for most of the events one can deduce that the excited electron is produced with a high degree of longitudinal polarisation. The excited fermions produced through only s–channel exchange, do not have a definite degree of polarisation. The transverse and longitudinal polarisations may be extracted from R_1 and R_2

$$P_{\parallel} = -\frac{(2-\beta)\cos^2\theta - \beta + 2A_2/A_1\,(1-\beta)\cos\theta}{2(1-\beta)+\beta(1-\cos^2\theta)+2A_2/A_1\,(1-\beta)\cos\theta}$$

[4]One can arrive at the same conclusions by considering the polarisation vector of the excited neutrino. The spin dependent term $n.p_2 \equiv n.(l_1+l_2)$ in eq. (3.17) shows that in the pure W exchange case, the excited neutrino is completely longitudinally polarised, $P_{\parallel}=+1$.

$$P_{\perp} = \frac{2m_*}{\sqrt{s}}\sin\theta\frac{\cos\theta + A_2/A_1}{2(1-\beta)+\beta(1-\cos^2\theta)+2A_2/A_1\,(1-\beta)\cos\theta} \qquad (3.18)$$

One observes that in the exact backward direction all excited fermions have $P_{\parallel}=-1$ [this also holds for the first generation excited fermions since the t–channel contributions vanish in this direction], whereas in the forward direction only the muonic excited fermions, μ^*, ν_μ^*, have $P_{\parallel}=-1$. In the case of the latter, a slight forward–backward asymmetry is present in the longitudinal polarisation due to the small interference terms between the axial and vector couplings at the e^+e^- vertex. For instance, in the case of the ν_μ^*, $P_{\parallel}$ is almost symmetric with respect to the scattering angle, with a maximum at $\theta=\pi/2$. At this angle, since the interference term vanishes, the μ^* and ν_μ^* have the same degree of longitudinal polarisation as seen from the figure, and is equal to the velocity of the fermion: $P_{\parallel}(\pi/2) = (s-m_*^2)/(s+m_*^2)$. On the other hand the value of the transverse degree of polarisation for this angle is a measure of the asymmetric term $P_{\perp}(\frac{\pi}{2}) = \frac{A_2}{A_1}\frac{2m_*}{\sqrt{s}}\frac{1}{1+m_*^2/s}$; were it not for the A_2 term , $P_{\perp}$ would have been odd around $\cos\theta=0$. Note that the transverse polarisation of the excited electron is always negative.

b) Total cross sections and signatures:

The total section for the single production of ν_e^*, which is the same for $\overline{\nu_e}\nu_e^*$, is found to be

$$\begin{aligned}\sigma &= \sigma_0\frac{3s}{4\Lambda^2}\beta\left\{(1-\frac{2}{3}\beta)\beta A_1^{\nu} + 4f_W^2 v_W^2\left[(2w+\beta)\log(1+\frac{\beta}{w})-2\beta\right]\right.\\ &+ \left. 4f_W v_W\left(e_e f_\gamma + \frac{a_e+v_e}{1-z}f_Z\right)\left[w(1+\frac{w}{\beta})\log(1+\frac{\beta}{w})-\frac{1}{2}(\beta+2w)\right]\right\} \qquad (3.19)\end{aligned}$$

This formula may be used for all other flavours except for the e^* by setting $f_W=0$ and by including the colour factor for quarks:

$$\sigma = N_c\;\sigma_0\;\frac{3s}{4\Lambda^2}\;\beta^2(1-\frac{2}{3}\beta)\;A_1^f \qquad (3.20)$$

To obtain the total cross-section in the case of the excited electron requires some care because of the t–channel photon exchange in the very forward direction. The electron mass terms must be kept and, besides the additional contribution of the R_6 term, the variable r in eq. (3.15) must be changed to include the electron mass. This is equivalent to integrating eq. (3.15) using the previous expression for r but with the scattering angle ranging over

$$-1 \le \cos\theta \le 1 - 2\frac{m_e^2}{s}\frac{(1-\beta)^2}{\beta^2} \qquad (3.21)$$

The expression for the total cross section including all contributions is very involved and not very telling. A very good approximation, as soon as one moves away from the Z–peak, is given by taking into account only the s and t–channel photon exchanges. Keeping the dependence in the electron mass in the leading terms, one obtains the simple expression

$$\sigma = \sigma_0\frac{3s}{4\Lambda^2}f_\gamma^2\;\beta\left[(1-\frac{2}{3}\beta)\beta-\beta-3+\frac{1+\beta^2}{\beta}\log\left(\frac{s}{m_e^2}\frac{\beta^2}{(1-\beta)^2}\right)\right] \qquad (3.22)$$

The total cross sections are shown in Fig. 7. As emphasized previously, due to the t–channel photon exchange, the largest production rate occurs for the excited electron. For both LEP200 and the 500 GeV NLC, the e^* cross section is two orders of magnitude larger than that of the μ^*, and remains almost constant as the mass increases until it sharply drops near threshold. The t–channel enhancement of the excited electronic neutrino production cross section is also important, especially at higher energies. For the other charged excited leptons, for which only s–channel gauge boson exchange is present, the cross section is proportional to β^2 and drops slowly with increasing excited fermion mass. Since we consider the case of the excited leptons with masses larger than 100 GeV [otherwise they can be pair produced at LEP200] they will decay into real W/Z bosons and light leptons.

Excited neutrinos can be searched for through their decays into charged leptons and W's which subsequently decay into jets. If the mass of the excited neutrino is not too close to the total energy, this gives rise to "one–sided" events where all the activity is restricted to one hemisphere. This hemisphere will contain an isolated lepton and a pair of jets with an invariant mass of M_W, while the other hemisphere contains the missing energy $I\!\!E = (s - m_{\nu^*}^2)/2\sqrt{s}$ carried by the neutrino at the production vertex. This signal seems to be background free. However, if the ν^* mass is close to the total energy, the one-sided event topology is lost and the amount of missing energy is small. This may be faked by the semi–leptonic decay of a W^+W^- pair production which is one of the most important reactions at LEP200 [$\sim$ 15 pb] and NLC [$\sim$ 7 pb] [28]. This background can however be reduced by looking for a peak in the invariant mass of the jet–jet–lepton system and by measuring the missing transverse momentum [reflecting the presence of the neutrino from the decay of one of the standard WW] .

The decay of the ν^* into Z bosons and light neutrinos result in final states with a pair of jets [or charged leptons], with an invariant mass of M_Z and a large amount of missing energy. These final states, although interesting, do not seem to be useful, especially since at best they correspond to only one third of all events. Furthermore, it is not clear how the mass of the excited neutrino can be reconstructed. The most obvious background comes from Z pair production [for which the cross section is approximately a tenth of that of W pair production] [28] with one Z decaying into neutrinos and the other Z into jets, although one can use the fact that the missing energy from ZZ events corresponds to the beam energy. Another common source of background, especially at the NLC, comes from $e^+e^- \to f\bar{f}\gamma$ with a very energetic photon which disappears along the beam pipe, leading to an apparent missing energy. However, a cut on the missing transverse momentum, which is present in the signal but not in the background, reduces the latter considerably. Finally at $\sqrt{s} = 500$ GeV, an important background comes from single W production via γW fusion, leading to a final $We\nu$ state with a cross-section $\sigma \simeq 5$ pb [29] where the electron escapes undetected and the neutrino carries missing transverse momentum. This background would be difficult to eliminate if the invariant mass of the jet pair is not accurately reconstructed, so that we do not know whether it originates from a W or a Z.

For the excited charged leptons, the electromagnetic decay stands as a clean signal, even if for large masses it accounts for only a third of all events. In the case of the μ^*, the events consist of an ordinary muon with energy $(s - m_{\mu^*}^2)/2\sqrt{s}$ recoiling against a muon and an energetic photon system of invariant mass m_{μ^*}. All three particles are well separated. The

background due to initial and final state radiation in $\mu^+\mu^-$ production should be easy to eliminate by imposing a cut on the photon energy and angle and look for a peak in the invariant mass of the $\mu\gamma$ system. Around the threshold for μ^* production, the ordinary muon at the production vertex is soft and may be undetected, but the $\mu\gamma$ pair from the μ^* decay would be unmistaken. Exploiting the decays into jets one has to fight against the background $e^+e^- \to W^+W^-$ leading to $\nu_\mu\mu$ jet-jet final states.

In the case of the excited electrons, the situation is quite different. Because the main contribution to the cross section comes from the t–channel photon exchange, the e^* is produced in the very forward direction and the accompanying positron is lost in the beam–pipe. Moreover, the e^* has $P_{||} = 1$ in this direction and combining this result with the polarised decay that we derived previously, the $e^* \to e\gamma$ occurs with an angular distribution

$$\frac{1}{\Gamma}\frac{\mathrm{d}\Gamma}{\mathrm{d}\cos\omega_e} \approx 1 + \cos\omega_e \qquad (3.23)$$

where ω_e is the angle of the e^- with respect to the electron beam, as viewed in the e^* rest frame. As it is known, the main background comes from radiative Bhabha scattering, $e^+e^- \to e^+e^-\gamma$. This background has been analysed for the LEP200 Workshop [15] and can be drastically reduced by requiring the photon to be very energetic, $E_\gamma > 0.2E_{\rm beam}$ and $E_{e^-} > 0.05E_{\rm beam}$ and by imposing an isolation cut on the $e\gamma$ angle. One then looks for a peak in the invariant mass of the observed $e\gamma$ system. The decay of the excited electron through $e^* \to W\nu$ does not seem to offer a better signal at the 500 GeV NLC since once again, single W production with a cross section of ~ 5 pb [29] swamps the signal. However one could improve the situation by reconstructing the angular distribution of the produced W in the e^* decay that one can derive along the lines of $e^* \to e\gamma$:

$$\frac{1}{\Gamma}\frac{\mathrm{d}\Gamma}{\mathrm{d}\cos\omega_W} \approx \frac{1 - \cos\omega_W + \mu^2(1 + \cos\omega_W)/2}{2 + \mu^2} \qquad (3.24)$$

where $\mu^2 = M_W^2/m_{e^*}^2$ and ω_W is the angle of the W^- with respect to the electron beam, as viewed in the e^* rest frame.

In Table 2, we display the discovery limits of excited leptons at LEP200 and the 500 GeV NLC. For the excited neutrinos we have only considered the decays into W's and charged leptons and required the observation of 20 events [corresponding to $\nu^*\bar{\nu}$ and $\bar{\nu}\nu^*$ production]. In the case of excited muons, the discovery limits are based on the observation of 20 events by taking into account the electromagnetic decays only. For excited electrons, because of the larger background, the limit is based on the observation of 40 events where one counts both e^{*+} and e^{*-}. The first observation is that in case of a negative search, the NLC will improve the bound on the scale Λ by about a factor 5 for all flavours when we compare the respective masses near to threshold. As expected, the strongest bounds are on the excited electron and on the excited electronic neutrino. For the e^*, the NLC can probe masses up to 450 GeV even for a scale $\Lambda/f \simeq 25$ TeV.

4 $e\gamma$ and $\gamma\gamma$ Collisions

Future high–energy e^+e^- linear colliders can be made to run in the $e\gamma$ or $\gamma\gamma$ mode by using Compton back scattering of laser light [13]. One then obtains $e\gamma$ colliders by converting only one of the initial electron or positron beams to a very energetic photon, or $\gamma\gamma$ colliders by converting both the electron and positron to photons. The $\gamma\gamma$ and $e\gamma$ luminosities will depend in a sensitive way on various machine parameters such as the polarisation of the original electron and laser beams, the distance from the convertion to the interaction point, etc [13]. Here we will assume, for simplicity, that the colliders have fixed center of mass energies $\sqrt{s_{e\gamma}} = 450$ GeV and $\sqrt{s_{\gamma\gamma}} = 400$ GeV and the same luminosities as the original e^+e^- collider. Since we give analytical formulae for cross sections and distributions, our analysis can be straightforwardly extended to take into account realistic photon spectra.

4.1 $e\gamma$ Collisions

a) e^* production

One of the best motivations for turning high–energy e^+e^- linear colliders into $e\gamma$ colliders is undoubtedly the search for excited electrons which can be produced as resonances in the s–channel; Fig. 8a. In this case, this mode of the collider would constitute an "e^* factory". The mechanism $e\gamma \to e^*$ has, in fact, already been encountered in the previous section since it can be viewed as the dominant subprocess in the reaction $e^+e^- \to e^+e^{*-}$ with the quasi–real photon given off by the e^+ beam. If there were no hint of the e^* from earlier searches [e.g. in the e^+e^- mode], one should in a first exploratory investigation choose the $e\gamma$ machine parameters to obtain a broad spectrum in order to localise the mass and then, one would tune these parameters to operate on the resonance peak. Since the excited electron has a very narrow width, the total cross section is very simply obtained by integrating over the Breit–Wigner resonance [30]

$$\sigma(\gamma e \to e^*) \;=\; \frac{8\pi^2}{m_{e^*}^2}\frac{\Gamma(e^* \to e\gamma)}{m_{e^*}} \;=\; \frac{2\pi^2\alpha}{\Lambda^2} f_\gamma^2 \tag{4.1}$$

This cross-section can be extremely large: for $\Lambda/f \sim 1$ TeV it is of $\mathcal{O}(50$ pb). To look for the e^* signal we will consider both its electromagnetic and weak decay into $W\nu_e$ since for large masses, this weak decay is twice as large as the photonic one [60% of all decays]. For both signals there are quite substantial backgrounds which we discuss in the following.

For $e^-\gamma \to e^* \to e^-\gamma$, the background comes mainly from Compton scattering, $e^-\gamma \to e^-\gamma$. However, the angular distribution of the final electron in this process is significantly different from the one resulting from the e^* decay. In the latter case, the distribution is readily obtained from the formulae of the polarised decays given in section 2 and in the Appendix, since the production cross section is directly related to the $e^* \to e\gamma$ decay. With the chiral form of the de–excitation couplings, the normalised distribution for the signal is

$$\frac{1}{\sigma}\frac{\mathrm{d}\sigma}{\mathrm{d}\cos\theta} = \frac{1+\cos\theta}{2} \tag{4.2}$$

where θ is the scattering angle of the electron i.e. the angle between the e^- beam and the final electron as measured in the e^* rest frame[6]. Therefore, the produced electron prefers the forward region[6], in contrast to Compton scattering where the electron flies opposite to the initial electron. Indeed, the differential cross section for this process is

$$\frac{\mathrm{d}\sigma}{\mathrm{d}\cos\theta} = \frac{\pi\alpha^2}{2s}\left[\frac{4}{1+\cos\theta+2m_e^2/s} + (1+\cos\theta)\right] \tag{4.3}$$

and is maximal for $\cos\theta = -1$. If no cuts are imposed, the total cross section is very large

$$\sigma = \frac{3\sigma_0}{4}\left[1 + 2\log\frac{s+m_e^2}{m_e^2}\right] \;\approx 20 \text{ pb} \;\text{ at }\; \sqrt{s} = 450 \text{ GeV} \tag{4.4}$$

One has, therefore, to cut as much as possible on the backward direction. Using the asymmetric cut $-0.7 \le \cos\theta \le 0.9$, only 8% of the background remains while 88% of the signal is retained. Requiring an observation of 10 $e^* \to e\gamma$ events over the $e\gamma \to e\gamma$ background, excited electrons with masses below the kinematically accessible limit [$\simeq 450$ GeV for a 500 GeV e^+e^- collider] can be discovered up to values of the scale Λ of about 120 TeV!

Before applying cuts, the signal $e^-\gamma \to e^* \to \nu W^-$ suffers from the even larger background from the process $e^-\gamma \to \nu W^-$ when $\sqrt{s} > 400$ GeV. As previously, it is straightforward to derive the distribution of the produced W^- emanating from the e^* decay

$$\frac{1}{\sigma}\frac{\mathrm{d}\sigma}{\mathrm{d}\cos\omega_W} = \frac{1-\cos\omega_W+\mu^2(1+\cos\omega_W)/2}{2+\mu^2}\;, \qquad \mu^2 \equiv \frac{M_W^2}{s} = \frac{M_W^2}{m_{e^*}^2} \tag{4.5}$$

where ω_W is the angle between the electron beam and the W^-. Defining $\beta_W = 1 - M_W^2/s$, the angular distribution of the νW^- background is given by [32]

$$\begin{aligned}\frac{\mathrm{d}\sigma}{\mathrm{d}\cos\omega_W} \;&=\; \frac{1}{2s}\frac{\pi\alpha^2}{4\sin^2\theta_W}\beta_W^2\frac{(1-\cos\omega_W)\,(4\beta_W^2+[2-\beta_W(1+\cos\omega_W)]^2)}{[1+\cos\omega_W+2(1-\beta_W)/\beta_W]^2} \\ &\xrightarrow{\beta_W\to 1} \frac{1}{2s}\frac{\pi\alpha^2}{4\sin^2\theta_W}\frac{1-\cos\omega_W}{(1+\cos\omega_W)^2}\left[4+(1-\cos\omega_W)^2\right]\end{aligned} \tag{4.6}$$

Therefore, for large e^* masses the W boson originating from the signal is produced in the opposite direction to the e^- beam, whereas the W from the background prefers the e^- direction at these high–energies. Removing the W's produced in the direction of the electron beam efficiently selects the signal events. Note that if one chooses for the W to decay into

[5] Renard has calculated the full $e^-\gamma \to e^-\gamma$ cross section, including the effect of the e^*, with a general transition coupling [30]. One can check, for the particular case of a transition involving only one chirality state of the ordinary fermion, that the contribution of the resonant term agrees with our simple formula.

[6] When refering to backward and forward scattering in an $e\gamma$ collider a note of caution is necessary. If the original e^+ and e^- beams have the same energy, one would end up with an asymmetric $e\gamma$ collider since the energy of the photon beam cannot exceed 90% of the to–be–converted beam. As a consequence, all products will be boosted in the initial e^- direction but one can easily correct for this feature if the photon beam is sufficiently monochromatic so that the total longitudinal momentum of the initial state is known. Another possibilty [31] is to arrange for the electron beam to have only 90% of the to–be–converted positron beam, so that the $e\gamma$ collider is a symmetric machine.

jets then the background from the process $e^-\gamma \to e^-Z$ has to be taken into account. This process has a large cross section and produces a Z boson along the electron beam [the accompanying e^- being lost in the beam-pipe] hence giving a topology of a pair of jets in the forward direction too. This background could be reduced by exploiting the fact that it produces missing energy but no large missing transverse momentum. Hence, the discovery limit given above and which is based only on the electromagnetic decays is conservative since one can also exploit the W decays.

b) ν^* production

We have also looked at the possibility of searching for the electronic excited neutrino in the $e\gamma$ mode[7]. The latter can be produced only in association with a charged W boson and therefore one can only probe masses below 370 GeV for a 450 GeV $e\gamma$ collider. However, it is not excluded that the ν^* is the lightest excited particle, and that the e^* is too heavy to be produced. In any case, the process is quite interesting to investigate as it directly probes the non-abelian structure of the transition couplings. The diagrams contributing to the $e\gamma \to \nu^* W^-$ process are displayed in Fig. 8b. Besides the diagram with the t-channel W exchange involving the standard non-abelian $WW\gamma$ vertex, there is also a diagram with a contact $e\gamma\nu^* W$ interaction which is crucial for gauge invariance. Indeed it is only with the inclusion of this latter diagram, that the amplitude is transverse in the photon momentum as it should be. The diagram where an e^* is exchanged in the s-channel is, on its own, transverse in the photon momentum [independently of the form of the $e^*\nu^* W$ coupling] and gives a vanishing contribution for very large e^* masses. However, for masses around the total energy, this contribution can be substantial since one is then close to the e^* resonance.

The differential cross section [of which the very lengthy analytic formula will not be given here] is displayed in Fig. 9a for several e^* masses. It is in general fairly flat, except for extreme values of the excited electron partner mass: when m_{e^*} is smaller than the total energy it slightly favours the forward direction [i.e., the W^- prefers the initial γ direction] while it vanishes in the exact forward direction for a very heavy e^*.

Using the variables $e = m_{e^*}^2/s, n = m_{\nu^*}^2/s, w = M_W^2/s$ and $\lambda = (1-n-w)^2 - 4nw$, the total cross section is given by

$$\begin{aligned}\sigma &= \frac{3}{4s_W^2}\frac{s}{\Lambda^2} f^2 \sigma_0 \lambda^{1/2} \left\{ \frac{e+1}{(e-1)^2}\left[\frac{(n-1)^2}{w} + n + 1 - 2w - \frac{12\sqrt{en}}{e+1}\right]\right. \\ &+ \frac{2}{e-1}\left[\frac{(1-n)(1+\sqrt{en})}{w} + 4n - 1 + 2w + \sqrt{en}(6w-6n-1)\right] \\ &+ \frac{n+1}{w} + 3n + w + 7(nw + w^2 - 2n^2 + n - 3) + \frac{4}{\lambda^{1/2}}\log\frac{1-n+w-\lambda^{1/2}}{1-n+w+\lambda^{1/2}} \\ &\times \left.\left[\frac{2n+3w\sqrt{en}+w}{e-1} + nw(1-3n) + 2n(2-n+n^2) + w(w^2+w-3) - 2\right]\right\} \quad (4.7)\end{aligned}$$

[7]This process has also been recently considered in ref. [33], but no analytical formulae have been given for the cross sections.

It is shown in Fig. 9b for various values of m_{e^*}. As one can see, the s-channel e^* exchange diagram can enhance the cross section by several orders of magnitude if the e^* mass is close to the total energy of the collider. The smallest cross section is obtained in the case of infinite m_{e^*}. However, even in this pessimistic case the cross section is about a factor of three larger than the one for single ν_e^* production in e^+e^- collisions up to masses of 350 GeV.

The decay $\nu^* \to e^- W^+$ would lead to the very clean final state consisting, if we restrict ourselves to the hadronic decays of the W's, of an isolated energetic electron and two pairs of jets with invariant masses $\bar{M}_W$. The bounds on Λ which are given in Table 2, are obtained in the pessimistic case of infinite m_{e^*}, and assume that 10 such events are observed with the same luminosity of 10 fb^{-1} as in the e^+e^- mode.

4.2 $\gamma\gamma$ collisions

While the $e\gamma$ mode discriminates between the first generation excited leptons and all the other excited fermions, the $\gamma\gamma$ mode obtained by converting both the e^+ and e^- beams into photons, is a more democratic means for single and double production of all charged excited fermions; Fig. 10. Compared to e^+e^- annihilation, this mode can serve to unambiguously isolate the purely electromagnetic part of the excited fermions couplings.

a) Pair Production

Using the general form of the $\gamma f\bar{f}$ coupling given in eq. (2.2) [the subscripts γ in f_1 and f_2 are suppressed for simplicity] and neglecting the double de-excitation contributions for the same reasons as for e^+e^- annihilation, the differential cross section for the process $\gamma\gamma \to \bar{f}f$ is

$$\frac{\mathrm{d}\sigma}{\mathrm{d}\cos\theta} = \sigma_0 N_c \frac{3}{2}\beta\left\{\frac{\mathrm{d}G_{11}}{\mathrm{d}\cos\theta} f_1^4 + \frac{\mathrm{d}G_{22}}{\mathrm{d}\cos\theta} f_2^4 + \left[(4f_1^2 + f_1 f_2 - 2f_2^2)\frac{\mathrm{d}G_{12}}{\mathrm{d}\cos\theta} + f_2(f_1+f_2)\frac{\mathrm{d}G_{21}}{\mathrm{d}\cos\theta}\right] f_1 f_2\right\} \quad (4.8)$$

with

$$\begin{aligned}\frac{\mathrm{d}G_{11}}{\mathrm{d}\cos\theta} &= 1 + \frac{2\beta^2}{1-\beta^2\cos^2\theta} - \frac{2\beta^4(1-\cos^2\theta)^2}{(1-\beta^2\cos^2\theta)^2} \quad , \quad \frac{\mathrm{d}G_{12}}{\mathrm{d}\cos\theta} = \frac{1}{1-\beta^2\cos^2\theta} \\ \frac{\mathrm{d}G_{22}}{\mathrm{d}\cos\theta} &= \frac{1-\beta^2\cos^2\theta}{4(1-\beta^2)^2} + \frac{\beta^2(1-\cos^2\theta)}{2(1-\beta^2)(1-\beta^2\cos^2\theta)} \quad , \quad \frac{\mathrm{d}G_{21}}{\mathrm{d}\cos\theta} = \frac{4}{1-\beta^2} \quad (4.9)\end{aligned}$$

Since the excited fermions are rather heavy there is only a very slight forward/backward peak for the usual point-like couplings. Once the mass of the excited fermion has been measured, the angular distribution can be used to see whether a magnetic form factor is present. Integrating over the scattering angle, the total cross section reads

$$\sigma = \sigma_0 N_c \frac{3}{2}\beta\left\{G'_{11} f_1^4 + G'_{22} f_2^4 + \left[(4f_1^2 + f_1 f_2 - 2f_2^2)G'_{12} + f_2(f_1+f_2)G'_{21}\right] f_1 f_2\right\} \quad (4.10)$$

with

$$\begin{aligned}G'_{11} &= \frac{1}{\beta}\left[(\beta^4 - 3)\log\frac{1-\beta}{1+\beta} + 2\beta(\beta^2 - 2)\right] \quad , \quad G'_{12} = -\frac{1}{\beta}\log\frac{1-\beta}{1+\beta} \\ G'_{22} &= \frac{1}{2\beta}\left[\log\frac{1-\beta}{1+\beta} + \frac{\beta}{(1-\beta^2)^2}(3 - \frac{7}{3}\beta^2)\right] \quad , \quad G'_{21} = \frac{8}{1-\beta^2} \quad (4.11)\end{aligned}$$

Setting $f_1 = e_f$ and $f_2 = 0$, the total cross section reduces to the familiar form

$$\sigma = \sigma_0 N_c \frac{3e_f^4}{2}\left[(\beta^4-3)\log\frac{1-\beta}{1+\beta} + 2\beta(\beta^2-2)\right] \tag{4.12}$$

The total cross section is shown in Fig. 11 for the case of excited charged leptons, assuming a fixed center of mass energy $\sqrt{s_{\gamma\gamma}} = 400$ GeV. Besides the usual case $f_1 = e_f, f_2 = 0$, we also show the cross section for $f_1 = e_f(1 + s/\Lambda^2), f_2 = m_*^2/\Lambda^2$ with $\Lambda = 1$ TeV to illustrate the effects of the form factors and anomalous magnetic moments. One can see that the cross sections are larger than in the e^+e^- mode: for $m_{e^*} = 150$ GeV, the enhancement factor is ~ 2. However, only smaller masses can be probed in $\gamma\gamma$ collisions due to the loss in energy. Note that for excited quarks, their fractional charge assignment is a penalizing factor and the cross sections are $N_c e_q^4$ times smaller than for a charged lepton of the same mass.

A most interesting signal for excited charged lepton production in $\gamma\gamma$ collisions will come from their electromagnetic decays, leading to two well separated and highly energetic photons [on average $E_\gamma \simeq E_{\rm beam}/4$] and isolated l^+l^- pairs. The background from $\gamma\gamma \to f\bar{f}\gamma\gamma$ is totally negligible, especially if one imposes isolation cuts on the four final particles. Another interesting channel, for l^* masses larger than M_W, is the one where an l^* decays electromagnetically while the other decays into $W\nu$, the W subsequently decaying into jets: one hemisphere would contain a jet pair and missing transverse energy while the other would contain a large angle lepton–photon pair. A possible background comes from radiative W pair production $\gamma\gamma \to W^+W^-\gamma$ followed by the semi–leptonic decay of the W [34]. However, this background turns out to be negligibly small when an isolation cut of $\cos\theta < 0.8$ on all final particles is made and if one requires the photon energy to be larger than 15 GeV : the background then contributes $\simeq 60$ fb while the signal cross section for $m_* = 150$ GeV would be $\simeq 1.5$ pb for point–like couplings. The final state where both excited leptons decay into W's suffers from the huge [~ 80 pb] [28, 35] background from $\gamma\gamma \to W^+W^-$, which is especially worrisome if the photon flux is not monochromatic, with the consequence that the missing energy from the signal can not be measured.

b) Single Production

All charged excited fermions can be singly produced in $\gamma\gamma$ collisions through two t–channel exchanges: one involving the partner light fermion and the other, the heavy excited fermion. Although both contributions are needed to insure gauge invariance, the light fermion exchange gives the dominant contribution. We encountered a similar t–channel enhancement with e^* production in e^+e^- collisions. Retaining the mass of the light fermions in the leading terms, the differential cross-section is given by

$$\frac{d\sigma}{dt} = 3N_c e_f^4 f^2 \frac{s}{\Lambda^2}\sigma_0\left\{3 + \frac{(1-a-2a^3)}{1+a}\frac{a}{t/s-a} - (1-2a+2a^2)\frac{a}{t/s-b} + \frac{2a^3}{(t/s-a)^2} + \frac{2a^2 b}{(t/s-b)^2}\right\} + \{t \longrightarrow u\} \tag{4.13}$$

with $a = m_*^2/s$, $b = m_f^2/s$ and where, retaining again the dependence in the mass of the light fermion, the Mendelstam variables t and u are given by

$$t/u = \frac{s}{2}\left[-(1-a)(1\mp x) + b\left(1 \mp \frac{1+a}{1-a}\right)\right] \tag{4.14}$$

The angular distribution for excited charged lepton production is shown in Fig. 12a for various m_* values. As one can see, it is forward/backward peaked, an effect which is more pronounced for the first generation leptons and, for a particular flavour, for smaller excited lepton masses. This mass effect almost disappears when a cut on the scattering angle is made on both the forward and backward direction. The total cross section is obtained by integrating t/s over the kinematically allowed range

$$-y(1-b)/b \le t/s \le -b + y/b$$

and, in agreement with the result given in ref. [18], is

$$\sigma = 6N_c e_f^4 f^2 \frac{s}{\Lambda^2}\sigma_0\left[a(2a^2-2a+1)\log\frac{(1-a)^2}{m_f^2/s} + \frac{a(1-a-2a^3)}{1+a}\log a + (1-a)(3+4a^2)\right] \tag{4.15}$$

It is displayed in Fig. 12b for the e^*, μ^*, τ^* leptons and with a cut on the scattering angle $|\cos\theta| < 0.8$. One notices that the cross section grows with the mass of the excited lepton almost up to threshold. Because of the light ordinary lepton mass effect, the cross section for a 300 GeV μ^* is only $\sim 60\%$ of that of an e^* with the same mass. With a cut–off $|\cos\theta| < 0.8$, these mass effects disappear and the cross section is the same for all lepton flavours. In the $\gamma\gamma$ mode, the cross sections for single l^* production are larger for all flavours [except for the e^* with a mass below 300 GeV] compared to the e^+e^- mode, even when the cut $|\cos\theta| \le 0.8$ is imposed.

For a clean signature, one has again to rely on the electromagnetic decays of the l^*. In this case the final state consists of a large invariant mass system formed by an energetic photon with a well separated charged lepton recoiling against missing energy [the accompanying lepton at the interaction point escaping detection]. An obvious background comes from $\gamma\gamma \to f\bar{f}\gamma$, but yet again, it can be drastically reduced by an isolation cut between the photon and one of the leptons. The decay $l^* \to W\nu \to \nu$–jet–jet gives also a clean final state. Note that in a machine where the conversion factor of the e^+/e^- beam into photons is not perfect [different from 1] one might get a contamination from the large standard model cross-section $e\gamma \to W\nu \to \nu$–jet–jet.

The discovery limits shown in Table 2 assume that 10 events based on the electromagnetic decay have been observed with an integrated luminosity $\mathcal{L}_{\gamma\gamma} = \mathcal{L}_{ee} = 10$ fb^{-1} using the electromagnetic decays only.

5 eP Collisions

As mentioned in the introduction, eP colliders are well suited for the search of the excited electron and its neutrino partner. The magnetic transition couplings of the electron to these first generation heavy leptons allows single production of e^* through t-channel γ and Z boson exchange and ν^* through t-channel W exchange [Fig. 13]

$$e^-(l_1)\ P(l_2) \longrightarrow V^*(q) \longrightarrow l^-(p_1)\ X(p_2) \tag{5.1}$$

Excited u and d quarks can also be produced in eP collisions [36] with sizeable rates. However, these states can be best probed in pp collisions [14] and will not be studied here.

5.1 Cross sections and distributions

The deep inelastic differential cross section for the process can be cast into the form

$$\frac{\mathrm{d}^2\sigma}{\mathrm{d}x\mathrm{d}y} = 2\pi\alpha^2\frac{s^2}{\Lambda^2}\,x^2y\,\sum_{q,\bar{q}}\left[A_l(Q^2)R(x,y)q(x,Q^2) + \bar{A}_l(Q^2)\bar{R}(x,y)\bar{q}(x,Q^2)\right] \tag{5.2}$$

where x is the momentum fraction of the proton carried by quarks or antiquarks, $y \equiv Q^2/(xs)$ [with $Q^2 \equiv -t = -(l_1 - p_1)^2$] and $\sqrt{s}$ is the energy in the eP center of mass frame. $q(x,Q^2)$ and $\bar{q}(x,Q^2)$ are the quark/antiquark structure functions, which we take from the parametrization given in ref. [37]. Taking into account the polarisation of the final heavy lepton, R and $\bar{R}$ are given by [$\mu_*^2 \equiv m_*^2/(xs)$]

$$\begin{aligned} R(x,y) &= 2 - (2-\mu_*^2)(y+\mu_*^2) + 2\mu_*/\sqrt{s}[\ n\cdot l_2 + (1-y-\mu_*^2)\ n\cdot p_2] \\ \bar{R}(x,y) &= \mu_*^2(2-y-\mu_*^2) + 2\mu_*/\sqrt{s}[\ n\cdot l_2 - (1-y-\mu_*^2)\ n\cdot p_2] \end{aligned} \tag{5.3}$$

and in terms of the quark couplings to the gauge bosons, A_l and $\bar{A}_l$ are defined by

$$\begin{aligned} A_\nu &= \bar{A}_\nu = f_W^2\frac{a_W^2+v_W^2}{(Q^2+M_W^2)^2} \\ A_e &= \frac{e_q^2 f_\gamma^2}{(Q^2)^2} + \frac{2e_q v_q^Z f_\gamma f_Z}{Q^2(Q^2+M_Z^2)} + \frac{[(v_q^Z)^2+(a_q^Z)^2)]f_Z^2}{(Q^2+M_Z^2)^2} \\ \bar{A}_e &= \frac{2e_q a_q^Z f_\gamma f_Z}{Q^2(Q^2+M_Z^2)} + \frac{2v_q^Z a_q^Z f_Z^2}{(Q^2+M_Z^2)^2} \end{aligned} \tag{5.4}$$

The corresponding cross section with an initial e^+ is simply obtained by $R(x,y) \leftrightarrow \bar{R}(x,y)$ in eq. (5.2). Note that in the unpolarised case, our formulae agree with those derived in ref. [9].

The parton cross-section eq. (5.2), is to be integrated over x and Q^2 to obtain the total deep–inelastic cross section,

$$\sigma(eP \to l^*X) = \int_{(m_*^2+Q_0^2)/s}^1 \mathrm{d}x \int_{Q_0^2/xs}^{1-\mu_*^2} \mathrm{d}y\ \ \frac{\mathrm{d}^2\sigma}{\mathrm{d}x\mathrm{d}y} \tag{5.5}$$

where the integration bounds are simply given by kinematics, upon taking into account a low Q^2 cut, $Q_0^2 \simeq 5$ GeV^2, which represents the limit of validity of the parton model.

In the case of e^* production, the t-channel photon exchange is very sensitive to very low Q^2 values which must be included. There is the contribution of the low Q^2 inelastic scattering [i.e. where the parton model is no longer valid] and the pure elastic scattering $eP \to e^*P$ [where the proton is lost in the tube]. Following the authors of ref. [9] but including the polarisation of the excited electron, the differential inelastic cross section [with photon exchange only] reads in terms of the usual electromagnetic structure functions of the proton F_1 and F_2

$$\begin{aligned} \frac{\mathrm{d}^2\sigma}{\mathrm{d}x\mathrm{d}y} &= \frac{\pi\alpha^2 f^2}{2\Lambda^2}\frac{1}{\beta_P^2 y}\left\{2F_1(x,Q^2)\left[(y+\mu_*^2)(2\mu_*^2-y) - 2\frac{(n.l_1)}{m_*}\mu_*^2(y+2\mu_*^2)\right]\right. \\ &+ \frac{1}{x}F_2(x,Q^2)\left[\left(4\beta_P^2 - (y+\mu_*^2)(4\beta_P - y + \frac{4M_P^2}{s}\frac{x}{y}\frac{\mu_*^2}{})\right)\right. \\ &+ \left.\left. 2\mu_*^2\frac{(n.l_1)}{m_*}\left(2\beta_P - y + \frac{4M_P^2}{s}\frac{x}{y}\frac{\mu_*^2}{}\right) + 4x\,\mu_*^2\frac{(n.l_2)}{m_*}(2\beta_P - y - \mu_*^2)\right]\right\} \end{aligned} \tag{5.6}$$

with $\beta_P \equiv 1 - M_P^2/s$ and the dimensionless variables y, μ_*^2 as previously defined. In this case however, $x \equiv Q^2/(W^2+Q^2-M_P^2)$, where in the low Q^2 inelastic case, W denotes the invariant mass of the final hadronic system while in the pure elastic case, $W^2 = M_P^2$ simply. Here again, we recover the result given in ref. [9] for the unpolarised case. For the elastic scattering the structure functions are given by

$$\begin{aligned} F_1(Q^2) &= \delta(W^2-M_P^2)\,\frac{Q^2}{2}\,G_M^2(Q^2) \\ F_2(Q^2) &= \delta(W^2-M_P^2)\,Q^2\left[G_E^2(Q^2) + \frac{Q^2}{4M_P^2}G_M^2(Q^2)\right]\left[1+\frac{Q^2}{4M_P^2}\right]^{-1} \end{aligned} \tag{5.7}$$

with the well known electric and magnetic form factors of the proton

$$G_E(Q^2) \simeq \frac{G_M(Q^2)}{2.79} \simeq \left[1 + \frac{Q^2}{(0.71\ \mathrm{GeV}^2)}\right]^{-2}. \tag{5.8}$$

In case the of the low Q^2 inelastic contribution, we follow the procedure outlined in [9], i.e. the proton structure functions are approximated by a fit of the type [38]

$$F_{1,2}(x,Q^2) \simeq \omega_W \sum_i b_{1,2}^i (1-1/\omega_W)^i \tag{5.9}$$

where $\omega_W = (W^2 - xQ^2)/(a_{1,2}^2 - Q^2)$, and the coefficients $a_{1,2}, b_{1,2}^i$ are fitted from low-Q^2 data [38].

The corresponding total cross sections are obtained by integrating the expression given in eq. (5.6) over the kinematically allowed range. For the elastic scattering case, the range is[8]

$$\frac{M_P^2}{s}\frac{m_*^4}{s-m_*^2} \le Q^2 \le s - m_*^2 \tag{5.10}$$

[8] Of course, the elastic cross section decreases so rapidly for high Q^2, that the precise value of the upper bound in eq. (5.10) is irrelevant in practice.

and is slightly more involved for the low-Q^2 inelastic contribution [the corresponding limits on x and y can be derived from the expressions given above]

$$(M_P + M_\pi)^2 \;\leq\; W^2 \;\leq M_P^2 - Q_0^2\,(1 - \frac{s}{m_*^2})$$
$$(\frac{m_*^2}{s})\left[W^2\left(1+\frac{m_*^2}{s}\right) - M_P^2\right] \;\leq\; Q^2 \;\leq\; Q_0^2 \qquad (5.11)$$

The total cross sections for e^* and ν^* production are shown in Fig. 14 for HERA [$\sqrt{s}$ = 314 GeV] and LEP/LHC [$\sqrt{s}$ = 1.26 TeV] energies and for $\Lambda/f = \Lambda/f' = 1$ TeV. For e^* production, the three different contributions discussed above are shown separately. Due to the low Q^2 t-channel photon exchange, the total e^* cross section is about one order of magnitude larger than for ν^* at HERA energy. At LEP/LHC energy, the cross section is about a factor two higher for e^* than for ν^*. For the former, it is important to note that the elastic contribution at HERA accounts for almost half of the total production rate and is more important for larger masses. This contribution is slightly reduced at LEP/LHC energies, although it still accounts for $30-40\%$ of all e^* production.

An observable which may help to characterize a signal for excited leptons and, as will be shown later, in reducing the background in the ν^* case, is the distribution of the transverse momentum of the final heavy state. This is the same as the transverse momentum of the scattered jet, P_T^{jet}, from the proton vertex. One obtains

$$\frac{\mathrm{d}\sigma}{\mathrm{d}P_T} = \int_{x_{\min}}^1 \mathrm{d}x\; \frac{\sqrt{xys\,(1-\mu_*^2-y)}}{(1-\mu_*^2-2y)}\;\; \frac{\mathrm{d}^2\sigma}{\mathrm{d}x\mathrm{d}y} \qquad (5.12)$$

where the lower integration bound is given by

$$x_{\min} = \frac{m_*^2}{s} + 2\frac{P_T^2}{s}\left[1+\sqrt{1+m_*^2/P_T^2}\,\right] \qquad (5.13)$$

In eq. (5.12), $\mathrm{d}^2\sigma/\mathrm{d}x\mathrm{d}y$ refers to the deep-inelastic contribution only, since the two additional contributions in the e^* case are only relevant for very small P_T. The obtained P_T spectrum is shown in Fig. 15 for ν^* [both at HERA and LEP/LHC] and in Fig. 16 for the e^* for three different e^* and ν^* masses. The shape of the P_T distribution is not extremely dependent on the mass although, of course, the maximal P_T value is smaller for larger masses.

The excited neutrinos have large transverse momenta in general. For instance, for a ν^* mass of 100 GeV, the average transverse momentum at HERA is $< P_T >= 50.7$ GeV. It is larger than for other types of exotic neutral leptons, as discussed for instance for the case of Majorana or mirror neutrinos [39]. It is also larger than for an excited electron of the same mass which has $< P_T >= 19$ GeV. This can be easily understood since

$$P_T^2 \equiv xys(1-\mu_*^2-y) \qquad (5.14)$$

reduces to $\simeq Q^2(1-\mu_*^2)$ for small Q^2, so that the low P_T values have higher probability in the e^* case where low Q^2 values dominate the cross section. The difference between the e^* and

ν^* is also reflected in the P_T spectrum, where low P_T are seen to be favoured in the e^* case at least for moderate m_* values. Essentially the same behaviour is observed at LEP/LHC energy, where of course higher P_T can be reached. This feature, together with the different y distributions, can help to disentangle excited heavy neutrals from other kinds of new leptons like e.g. those expected to appear in extended gauge models [39]. For the excited electrons the distinction can readily be made because of the large electromagnetic branching ratio.

An additional means to characterize excited leptons is their final polarisation. The polarisation vector P_μ of the final excited fermion is defined as in e^+e^- collisions

$$\mathrm{d}\sigma^{\mathrm{pol}}(Q^2) = \mathrm{d}\sigma^{\mathrm{unpol}}(Q^2) \times [1 + P_\mu n^\mu] \qquad (5.15)$$

The longitudinal $P_\parallel$ and transverse $P_\perp$ components of the e^* and ν^* polarisation vectors are shown as a function of the momentum transfer in Fig. 17 for $m_* = 100$ GeV at HERA and $m_* = 300$ GeV at LEP/LHC. The difference between the polarisation vector components of the e^* and ν^* are very small and do not appear at the scale of the figure. This comes from the fact that in electron proton collisions the contribution of antiquarks comes only from the sea quarks, and is thus very much suppressed with respect to the contribution of valence quarks. Therefore, due to the same chiral structure which appear in both the e^* and ν^* in the t-channel production, the normalised polarisation vector is the same. This can be seen from eq. (5.2) by neglecting the antiquark contribution, which would then mean that the polarisation vectors are given by $R(x,y)$ irrespective of the strength of the coupling A_l. For very low or very large values of the momentum transfer Q^2, the states are completely longitudinally polarised. $P_\parallel$ increases from -1 to $+1$ with increasing Q^2 while $P_\perp$ is always positive and rather large for intermediate Q^2 values. By integrating over Q^2 [and x], the components of the total polarisation vectors are obtained. In the case of HERA and for an excited lepton mass of 100 GeV the values are $P_\parallel^{\mathrm{tot}} = -0.46$ and $P_\perp^{\mathrm{tot}} = 0.48$.

5.2 Signals and backgrounds

a) Excited electrons

In view of the fact that almost half of all the excited electrons are produced in the elastic channel, at very low Q^2 where the proton may be regarded as giving off an almost real photon and diseappearing undetected in the beam pipe, the electromagnetic decay $e^* \to e\gamma$ is the best channel to reveal the presence of the e^*. Indeed, this leads to very "quiet" events with a wide angle and energetic electron-photon pair. The main background, coming from the bremsstrahlung process $eP \to eP\gamma$ [40], can be significantly reduced by imposing a cut on the energy of the photon and by demanding that the electron and the photon be emitted at large angles. Moreover, one could require the invariant mass of the $e\gamma$ system to be above 90 GeV at HERA [which is the limit set by LEP1 on the e^* mass] and 150 GeV, say, at LEP/LHC. Note that the electrons from the decay product of the e^* and from the background are preferentially emitted in opposite directions[9]. Note also that, as pointed out by

[9] See for instance our discussion of e^* production in $e\gamma$ collisions. In fact, in the elastic case, the main contribution has as its dominant subprocess $e\gamma \to e^*$ which should be convoluted with the photon flux coming from the proton.

Carli [41], the deep–inelastic background with the photon produced from the hadronic jet [e.g. π decay] poses no problem for an invariant $M_{e\gamma}$ mass above 80 GeV.

For the elastic e^* production, it could also be interesting to exploit the decay $e^* \to \nu W$. In order to avoid the very large background from the QCD induced 2 jets events [which is important even after imposing P_T cuts on both jets and on their invariant mass], we will only consider the subsequent decays of the W into muons. For an e^* mass of 150 GeV, this corresponds to a combined branching ratio of 7%. Although this sample constitutes about a quarter of the electromagnetic decays, it is rather interesting since it leads also to "quiet" final state events with an energetic muon and a large amount of missing transverse energy. The background from elastic single production of the W [42] which decays into $\nu\mu$ pairs is negligible at HERA [the cross section $\sim 2.10^{-3}$ pb, gives less than one event assuming an integrated luminosity of 200 pb^{-1}] while it is small at LEP/LHC [the larger cross section 5.10^{-2} pb leads to about 50 isolated muons with the anticipated 10^3 pb^{-1} integrated luminosity]. Even at LEP/LHC one could enhance the signal by taking into account the different distributions of the W produced from the e^* and the one produced through single W production, as discussed in the $e\gamma$ section.

Requiring 10 e^* events through the $e\gamma$ identification, masses up to 160 GeV can be probed at HERA with an integrated luminosity of 200 pb^{-1} and up to 850 GeV at LEP/LHC with an integrated luminosity of 10^3 pb^{-1}, provided that $\Lambda/f \approx 1$ TeV. If the compositeness scale is at $\Lambda/f \approx 2$ TeV, then HERA will only be able to probe excited electron masses below 100 GeV. Likewise, if the scale Λ is set at 4 TeV, then LEP/LHC will probe excited electron masses up to 400 GeV. These values are in agreement with those obtained in [17].

b) Excited neutrinos

The excited ν_e^* can be looked for through its decay into an electron and a W^+. The subsequent decay of this W into jets suffers from a large background due to photoproduction of jets [43] which incidentally is the same background to single W production. Although by requiring large P_T cuts on all the jets and the electron and by enforcing the invariant mass of a jet pair to form the W mass, it seems difficult to reduce this background to the level where it clearly stands above the signal. For this reason it would be preferable to only rely on the leptonic decays $W \to e\nu_e, \mu\nu_\mu$ which account for approximately 1/5 of the $\nu^* \to W^+e^-$ events. Although there is a missing P_T, the kinematics is well constrained enabling a ν^* mass reconstruction. Tagging through the leptonic decays of the W, the only background to worry about is single W production. Since the charge of the W is given by that of the corresponding e^+ or μ^+ lepton, we only have to take into account e^-W^+ production, while, had we used jets, both e^-W^+ and e^-W^- backgrounds would have had to be considered.

At HERA energies, the cross section for single weak boson production is small[10] $\sigma(e^-W^+X) \simeq$ 0.6 pb [42, 44]. This leads to about 30 events of the type $e^-(e^+/\mu^+)$ jet-X and missing P_T.

[10]Various authors [42, 44] quote slightly different values due to different choices of scales in the Weizsäcker-Williams splitting functions, the regularisation of fermion poles, various proton structure functions, etc. For a very recent analysis see [42]. The values we quote are from this last reference and serve only as a guide.

This could be reduced further since single W^+ production, contrary to the ν^* case, occurs mainly at very low Q^2 [where here Q^2 is the usual one, i.e. as measured through the energy E_e and angle θ of the scattered electron: $Q^2_{\rm meas} = E_{e^-}^{\rm beam} E_e \sin^2(\theta/2)$]. Alternatively, a P_T cut on the scattered jet reduces single W production since the excited neutrino gives large $P_T^{\rm jet}$ as discussed above. Requiring the observation of 10 events, excited neutrinos with masses up to 150 GeV could be observed provided the scale Λ/f is below 300 GeV while a scale of 0.5 TeV could be probed for an excited neutrino with a mass of 100 GeV at HERA.

The decay of the excited neutrino through a Z which subsequently decays into neutrinos, leading to a large amount of unbalanced P_T and only one jet with a large P_T is almost background free, since single Z production at HERA has been calculated to be only 4. 10^{-3} pb [42]. Requiring four signal events of this type would lead to the same bounds as those set through the W decays.

At LEP/LHC, the search strategy for the ν^* should rely on the same topologies as at HERA: $\nu^* \to e^-W^+ \to e^-(\mu^+/e^+)\nu$ so that only single W production should be considered as a potential background. Here, however, the cross-section is large [45]: $\sigma(eP \to e^-W^+{\rm jet}) \simeq 14$ pb. Nonetheless, from the remarks made above for this reaction, it can be reduced substantially by Q^2 and $P_T^{\rm jet}$ cuts. The authors of reference [45] have given the distribution in the $P_T^{\rm jet}$ where we see that the bulk of the contribution comes from very low P_T values. We estimate that a cut of 50 GeV leaves about only 5% of the background whereas one retains as much as 80% of the signal from a 600 GeV ν^*. Requiring 20 signal events, excited electronic neutrinos with masses as high as 700 GeV can be probed with a scale $\Lambda/f \simeq 1$ TeV, and an excited neutrino with a mass of 400 GeV can be discovered for a compositeness scale up to 2 TeV.

Decays through the Z do not seem to help much at LEP/LHC, since, although the cross section for single Z production is small, $\sigma = 0.6$ pb, [42] it can not be reduced further because the P_T spectrum of the scattered jet is, as for the signal, broad [45]. Moreover, these decays of the ν^* represent a smaller fraction than the decays into W bosons.

6 Conclusions

Excited fermions constitute a direct reflection of a possible new layer of matter, and are an integral part of the new particles search programmes at present and future colliders. In this paper, we have analysed the production mechanisms and signatures of excited leptons at e^+e^- and eP colliders. e^+e^- machines are ideal instruments to search for such particles, since, besides the fact that they provide a clean environment for their detection, the initial state shares some of the quantum numbers of the excited particles of the first generation leading to specific production mechanisms. Furthermore, currently discussed future high–energy linear colliders will have the added benefit of running as high-energy $e\gamma$ and $\gamma\gamma$ colliders, the former being a potential e^* factory while the latter is a democratic means for producing all charged new particles. eP colliders also offer interesting possibilities in the search for the first generation of excited particles.

We have given complete and compact formulae for the decay widths of the excited fermions, their production cross sections and angular distributions, and analysed in some details the spin–dependence of the decays and the differential cross sections in the case of e^+e^- annihilation and eP collisions. Our results may help in setting Monte Carlo programs based on the factorisation of the production and decay sequences, which will allow for an easy reconstruction of the correlations between the initial state and the final products of the excited heavy states. We have discussed the various signals and backgrounds for the detection of these new particles, and estimated the masses and the compositeness scale which can be probed at the various machines that we have studied: LEP100 and LEP200, the NLC with the three modes e^+e^- at $\sqrt{s} = 500$ GeV, $e\gamma$ at $\sqrt{s} = 450$ GeV and $\gamma\gamma$ at $\sqrt{s} = 400$ GeV, as well as the eP colliders HERA and LEP/LHC. Our results for the discovery potentials of these machines are summarized in Table 2; these numbers are only an estimate and detailed Monte Carlo analyses which take into account specificities of particular detectors are needed to obtain more precise values.

A common feature of the next colliders with respect to the first generation excited leptons, is the prominent rôle played by t–channel boson exchange mechanisms, especially as concerns e^* production. Indeed, the subprocess $e\gamma \to e^*$ is operative in both e^+e^- and eP collisions, generating large production rates, which lead to very strong limits on the compositeness scale in case of a negative search. It also acts as one of the best motivations for running in the $e\gamma$ mode, since the e^* could be produced as a resonance; the absence of such a resonance for excited electron masses below the center of mass energy would lead to a bound as high as 120 TeV on the scale Λ. The $e\gamma$ mode is also favorable for the production of the excited electronic neutrino, if kinematically allowed: Λ scales of the order of 25 TeV can be probed for masses below 350 GeV at a 450 GeV $e\gamma$ collider. The second generation excited charged and neutral leptons can be produced in e^+e^- collisions, up to masses close to the total center of mass energy if Λ is less than 2 TeV. For the charged leptons, as compared to the e^+e^- mode, one can reach a much higher scale in the $\gamma\gamma$ mode where the t–channel enhancement is also effective for these two generations; though slightly smaller masses can be probed due to the loss in energy when converting the initial electrons beams to photons.

Finally, although eP colliders are not very sensitive to high values of the compositeness scale, they can probe large excited lepton masses for $\Lambda \sim 1$ TeV. Indeed, for the latter value of Λ, e^* masses up to 150 GeV are opened to HERA, while LEP/LHC can probe masses up to 850 GeV for e^* and 700 GeV for ν_e^*. These masses are larger than the corresponding ones which can be reached at LEP100 and the 500 GeV e^+e^- collider.

Acknowledgments: We would like to thank F. M. Renard for a clarification about the $\nu*$ contribution to $g-2$. We have benefited from stimulating discussions with Ch. Berger, F. M. Renard and P. Zerwas as well as clarifying exchanges with E. Boos and I. Ginzburg. We would also like to thank T. Carli for discussions on the excited lepton searches at HERA and the ALEPH compositeness group, and in particular M. Bardadin-Otwinowska, for stimulating discussions on excited fermion searches at LEP.

APPENDIX: Final spin dependent differential decays and cross-sections

In this appendix, we give a simple formalism to describe the production of heavy fermions with their subsequent decays including the spin correlations, and show how it can be used for excited fermion production. We consider only the case of e^+e^- scattering, the generalisation to the case of eP scattering being straightforward.

a) Longitudinal and transverse degrees of polarisation

To define the components of the polarisation vectors, we choose the (z,x) plane as the scattering plane, with the e^- along the $+z$ direction. The f^* four momentum is defined as $p_\mu = (E, \vec{p}\,)$. The covariant spin vector n_μ satisfies the relations $n.n = -1$, $n.p = 0$. A general state of polarisation can be decomposed along three directions: the f^* direction $\vec{p}$ ($\vec{n_\parallel}$), the transverse direction with respect to $\vec{p}$ but within the scattering plane ($\vec{n_\perp}$) and along a normal to the scattering plane ($n_N = \vec{p} \times \vec{n}/|\vec{p}|$). The projection of the spin vector along these three directions defines the corresponding degrees of polarisation:

$$n^\mu = P_\perp\, n_\perp^\mu + P_N\, n_N^\mu + P_\parallel\, n_\parallel^\mu \qquad \text{(A. 1)}$$

with

$$n_\parallel^\mu = \frac{1}{m_*}\left(|\vec{p}|, E\frac{\vec{p}}{|\vec{p}|}\right) \qquad n_\perp^\mu = (0, \vec{n_\perp}) \qquad n_N^\mu = (0, \vec{n_N}) \qquad \text{(A. 2)}$$

Note that all three vectors satisfy $n_i.p = 0$, $n_i.n_i = -1$. Since for the process at hand there is no CP violation and that we neglect the very small imaginary parts from width effects, there can be no polarisation transverse to the scattering plane, i.e. $P_N = 0$. Thus, we can set the azimuthal angle to zero and take $p_\mu = (E, p\sin\theta, 0, p\cos\theta)$ where θ is the scattering angle. Then $n_\perp = (0, \cos\theta, 0, -\sin\theta)$. The degrees of polarisation from the polarised production cross section

$$\mathrm{d}\sigma^{\mathrm{pol}} = \mathrm{d}\sigma^{\mathrm{unpol}}(1 + n.\mathcal{P}) \qquad \text{(A. 3)}$$

are simply

$$P_\parallel = n_\parallel.\mathcal{P} \quad \text{and} \quad P_\perp = n_\perp.\mathcal{P} \qquad \text{(A. 4)}$$

b) Factorisation

For single production of heavy particles, we follow the work of Tsai [46]. One first writes the differential cross section and the differential decay transition with the explicit spin dependence:

$$\begin{aligned} \mathrm{d}\sigma^{\mathrm{pol}}_{i\to f^*} &= \mathrm{d}\sigma^{\mathrm{unpol}}(1 + n.\mathcal{P}) \\ \mathrm{d}\Gamma^{\mathrm{pol}}_{f^*\to \mathrm{final}} &= \frac{1}{2}\mathrm{d}\Gamma^{\mathrm{unpol}}(1 + n.\mathcal{P}') \end{aligned} \qquad \text{(A. 5)}$$

In the narrow width approximation [which is an excellent approximation in the case of the excited fermions we study], the differential cross section for the production and subsequent decay of the fermion can be written as

$$\mathrm{d}\sigma_{i\to \mathrm{final}} = \mathrm{d}\sigma^{\mathrm{unpol}} \frac{\mathrm{d}\Gamma^{\mathrm{unpol}}}{\Gamma_{\mathrm{tot}}} \left(1 + \eta_{\mu\nu}\mathcal{P}^\mu\mathcal{P}'^\nu\right) \qquad \text{(A. 6)}$$

with

$$\eta_{\mu\nu} = -(g_{\mu\nu} - \frac{p_\mu p_\nu}{m_*^2}) \qquad \text{(A. 7)}$$

Note that $\eta_{\mu\nu}\mathcal{P}^\mu\mathcal{P}'^\nu = \vec{\mathcal{P}}^*.\vec{\mathcal{P}}'^*$, where the * refers to the components in the rest frame of the excited fermion. One can see that the above formalism is very well adapted for the setting of a very compact Monte Carlo generator including all possible correlations between the initial and the final particles from the decay of the excited fermion.

The previous formalism can be easily generalised to the case of pair production of a heavy fermion anti–fermion pair. Denoting the antiparticle spin vector by $\overline{n}$, the polarised cross section for the pair production is

$$\mathrm{d}\sigma^{\mathrm{pol}} = \mathrm{d}\sigma^{\mathrm{unp}}\left(1 + \mathcal{P}.n + \overline{\mathcal{P}}.\overline{n} + C^{\mu\nu}n_\mu\overline{n}_\nu\right) \qquad \text{(A. 8)}$$

Summing over the spin of the anti–fermion, for example, the last two terms disappear. The full cross section with the final decay products of the excited fermions writes [$\mathcal{P}'$ refers to the vector defined in the polarised decay] we have

$$\mathrm{d}\sigma = \mathrm{d}\sigma^{\mathrm{unpol}}\frac{\mathrm{d}\Gamma^{\mathrm{unpol}}}{\Gamma_{\mathrm{tot}}}\frac{\mathrm{d}\overline{\Gamma}^{\mathrm{unpol}}}{\Gamma_{\mathrm{tot}}}\left(1 + \eta_{\mu\nu}\,\mathcal{P}^\mu\mathcal{P}'^\nu + \overline{\eta}_{\mu\nu}\overline{\mathcal{P}}^\mu\overline{\mathcal{P}}'^\nu + \eta_{\mu\alpha}\overline{\eta}_{\nu\beta}C^{\mu\nu}\mathcal{P}'^\alpha\overline{\mathcal{P}}'^\beta\right) \qquad \text{(A. 9)}$$

where the tensor $\overline{\eta}_{\mu\nu}$ is defined as in (A.7) with $p \to \overline{p}$ the momentum of the anti–fermion.

c) Spin dependence and the chiral structure

To introduce the spin dependence, we simply replace the projection operators by

$$u(p)\overline{u}(p) \to \frac{1}{2}(\not{p} + m_*)(1 + \gamma_5\not{n}) \qquad \text{(A. 10)}$$

for particles. While for antiparticles

$$v(p)\overline{v}(p) \to \frac{1}{2}(\not{p} - m_*)(1 + \gamma_5\not{n}) \qquad \text{(A. 11)}$$

For single excited fermion production, because of the chiral couplings assumed, we always have to calculate a trace of the form

$$\mathrm{Tr}(\not{p} + m_*)(1 + \gamma_5\not{n})(1 - \gamma_5)(\Gamma^{\mathrm{odd}} + m_f\Gamma^{\mathrm{even}}) \qquad \text{(A. 12)}$$

where Γ^{odd} and Γ^{even} stand respectively for a string of an odd number and an even number of γ matrices. m_f is the mass of the ordinary fermion coupling to the excited fermion. m_f can always be safely neglected apart from the case of e^* production through a t–channel photon exchange. With this proviso, the trace reduces to

$$\mathrm{Tr}(\not{p} + m_*)(1 + \gamma_5\not{n})(1 - \gamma_5)\Gamma^{\mathrm{odd}} \qquad \text{(A. 13)}$$

Therefore the unpolarised cross sections can be derived from the polarised ones by setting $m_*\not{n} \to +\not{p}$ for particles and $m_* \to -m_*$, $m_*\not{n} \to +\not{p}$ for anti–particles. This is explicit in our formulae.

References

[1] F. Low, Phys. Rev. Lett. **14** (1965) 238.

[2] For reviews on substructure in the fermionic sector, see:
M. Peskin, Proc. of the 10th Int. Symp. on Lepton–Photon Interactions at High–Energies, Bonn FRG, August 1981;
H. Terazawa, Proc. of the Europhysics Topical Conference on Flavor Mixing in Weak Interactions, Erice Italy, March 1984;
W. Buchmüller, Lectures given at the 24th Int. Wochenuniversität für Kernphysik, Schladmig Austria, Feb. 1985;
R. Peccei, Proc. of the Lake Louise Winter Institute, Lake Louise Canada, Feb. 1987;
F. Boudjema, Int. J. Mod. Phys. **A6** (1991) 1.

[3] C. Bétourné et al., Phys. Lett. **17** (1965) 70;
H.J. Behrend et al., Phys. Rev. Lett. **15** (1965) 900.

[4] ALEPH Coll., D. Decamp et al., Phys. Lett. **B250** (1990) 172;
ALEPH Coll., D. Decamp et al., CERN-PPE/91-149, submitted to Physics Reports.

[5] L3 Collaboration, B. Adeva et al., Phys. Lett. **B252** (1990) 525.

[6] M. Davier, Rapporteur talk at the Lepton/Photon Conference, Geneva 1991, Preprint LAL 91-48, to appear in the proceedings;
M. Bardadin-Otwinowska, Z. Phys. **C55** (1992) 163.

[7] N. Cabibbo, L. Maiani and Y. Srivastava, Phys. Lett. **139B** (1984) 459.

[8] J. Kühn and P.M. Zerwas, Phys. Lett. **147B** (1984) 189.

[9] K. Hagiwara, S. Komamyia and D. Zeppenfeld, Z. Phys. **C29** (1985) 115.

[10] F. Boudjema and A. Djouadi, Phys. Lett. **B240** (1990) 485.

[11] Workshop on "Physics and Experiments with Linear Colliders", Saariselkä Finland, Sept. 1991, proceedings to appear (R. Orava, ed.).

[12] Workshop on "e^+e^- Collisions at 500 GeV: the Physics Potential", DESY Hamburg, Sept. 1991, proceedings to appear (P. M. Zerwas, ed.).

[13] C. Akerlof, University of Michigan Report UMHE 81–59;
I.F. Ginzburg et al., Nucl. Instrum. Meth. **205** (1983) 47;
V.I. Telnov, Nucl. Instrum. Meth. **A294** (1990) 72 (1983) 47;
see also the talks given by D. Borden, V. Telnov, B. Wiik in [11] and F. Richard in [12].

[14] U. Baur, I. Hinchliffe and D. Zeppenfeld, Int. J. Mod. Phys. A2 (1987) 1285;
U. Baur, M. Spira and P.M. Zerwas, Phys. Rev. **D42** (1990) 815.

[15] D. Treille [conv.] et al, ECFA Workshop on LEP200, Aachen, 1986, CERN 87–08.

[16] F.A. Berends and P.H. Daverveldt, Nucl. Phys. **B272** (1986) 131;
R. Kleiss and P. Zerwas, Proc. of Work. on Future Colliders, La Thuile, CERN 88-09;
F. Boudjema, F. M. Renard [conv.] et al., Z Physics at LEP 1, G. Altarelli, R. Kleiss and C. Verzegnassi, eds, CERN 89-08, Vol II (1989) p. 185;
M. Martinez, R. Miquel and C. Mana, Z. Phys. **C46** (1990) 637.

[17] Ch. Berger, J. Tutas and P. Zerwas, Proceedings of the HERA Workshop, R.D. Peccei ed., Vol II, DESY-88, p. 813;
Ch. Berger et al., in Proceedings of the LHC Workshop, Vol. 2 , p. 1014, CERN 90-10/ECFA 90-133, G. Jarlskog and D. Rein eds.

[18] I.F. Ginzburg and D. Yu. Ivanov, Phys. Lett. **B 276** (1992) 214.

[19] S.J. Brodsky and S.D. Drell, Phys. Rev. **D22** (1980) 2236.

[20] F.M. Renard, Phys. Lett. **116B** (1982) 264.

[21] A. Djouadi, D. Schaile and C. Verzegnassi [conv.] et al. in [12].

[22] Proceedings of the Workshop High Luminosities at LEP, CERN Report 91–02, E. Blucher et al., eds.

[23] OPAL Coll., M. Akrawy et al., Phys. Lett. **B257** (1991) 531.

[24] CELLO Coll., H.J. Behrend, Phys. Lett. **168B** (1986) 420.

[25] P. Méry, S.E. Moubarik, M. Perrottet and F.M. Renard, Z. Phys. **C46** (1990) 229.

[26] F. Boudjema and C. Hamzaoui, Phys. Rev. **D43** (1991) 3748.

[27] J. Kühn, A. Reiter and P. Zerwas, Nucl. Phys. **B272** (1986) 560.

[28] F. Boudjema, F.M. Renard [conv.] et al., ENSLAPP-A-365/92 to appear in [12].

[29] K. Hagiwara et al., Nucl. Phys. **365** (1991) 544.

[30] F.M. Renard, Z. Phys. **C14** (1982) 209.

[31] D.L. Borden, D.A. Bauer and D.O. Caldwell, Preprint USCB-HEP-92-01.

[32] E. Yehudai, Phys. Rev. **D44** (1991) 3434.
E. Yehudai, Ph.D. thesis, August 1991, SLAC-383.

[33] A. Beliaev, E. Boos and A. Pukhov, MPI-Ph/92-19, March, 1992.

[34] M. Baillargeon and F. Boudjema, Preprint ENSLAPP–A–400/92.

[35] I. F. Ginzburg el al., Nucl. Phys. **B228** (1983) 285;
For a recent analysis, see E. Yehudai, Phys. Rev. **D41** (1990) 33.

[36] G. Jikia, Nucl. Phys. **B333** (1990) 317.

[37] D. Duke and J.F. Owens, Phys. Rev. **D30** (1984) 49.

[38] F.W. Brasse et al., Nucl. Phys. **B39** (1972) 421.

[39] W. Buchmüller and C. Greub, Phys. Lett. **B256** (1991) 465; Nucl. Phys. **B363** (1991) 345;
F. Csikor and I. Montvay Phys. Lett. **B231** (1989) 503;
F. Csikor, Z. Phys. **49** (1991) 129.

[40] A. Courau and P. Kessler, Phys. Rev. **D33** (1986) 2028;
K.J.F. Gaemers and M. van der Horst, Nucl. Phys. **B316** (1989) 289. E **B336** (1990) 184.

[41] T. Carli, Ph. D Thesis, Ecole Polytechnique Paris, 1992;
T. Carli, P. Dingus and Y. Sirois, X-LPNHE/92-2.

[42] U. Baur, J.A.M. Vermaseren and D. Zeppenfeld, Nucl. Phys. **B375** (1992) 3.

[43] H. Baer, J. Ohnemus and D. Zeppenfeld, Z. Phys. **C43** (1989) 675.

[44] E. Gabrielli, Mod. Phys. Lett. A1 (1986) 465;
M. Böhm and A. Rosado, Z. Phys. **C34** (1987) 117, ibid **C39** (1988) 275;
C.S. Kim and W.J. Stirling, DTP/91/22, Durham Preprint, May 1991.

[45] U. Baur et al., in Proceedings of the LHC Workshop, Aachen FRG, p. 958, Vol. II, CERN 90-10/ECFA 90-133 (1990) G. Jarlskog and D. Rein, eds.

[46] Y.S. Tsai, Phys. Rev. **D4** (1971) 2821;
S. Kawasaki, T. Shirafuji and Y.S. Tsai, Prog. Theor. Phys. **49** (1973) 1656.

Table Captions

Tab. 1 Branching ratios and total decay widths of excited leptons: (a) excited neutrinos with masses below and close to M_Z for $f = 1.025$, $f' = 0.975$ (first columns) and for $f = f' = 1$ (second columns); (b) excited neutrinos with masses larger than M_Z and for $f = f' = 1$; (c) excited charged leptons for $f = f' = 1$. For the total widths, Λ is taken to be 1 TeV.

Tab. 2 Discovery limits of excited leptons at the various machines that we have studied (see text): present limits at LEP100, LEP200, the NLC in the modes e^+e^- with $\sqrt{s} =$ 500 GeV, $e\gamma$ with $\sqrt{s} = 450$ GeV and $\gamma\gamma$ with $\sqrt{s} = 400$ GeV, and the eP colliders HERA with $\sqrt{s} = 314$ GeV and LEP/LHC with $\sqrt{s} = 1.26$ TeV.

Figure Captions

Fig. 1 Feynman diagrams for the decays of excited charged and neutral leptons: $l^* \to lZ \to l\bar{f}f$, $l^* \to l'W \to l'\bar{f}'f$ and $l^* \to l\gamma$.

Fig. 2 Feynman diagrams for excited charged and neutral lepton production in e^+e^- collisions. a) pair production and b) single production.

Fig. 3 Total cross sections [in fb] for the pair production of excited charged and neutral leptons in e^+e^- annihilation as a function of the l^* mass. The full lines are for the usual vector couplings and the dashed lines include the effects of form factors: $f_1 = v^V(1 + s/\Lambda^2)$ and $f_2 = m_*^2/\Lambda^2$ with $\Lambda = 1$ TeV. (a) $\sqrt{s} = 200$ GeV and (b) $\sqrt{s} = 500$ GeV.

Fig. 4 Longitudinal and transverse polarisations of the excited lepton in pair production in e^+e^- collisions, as a function of the scattering angle and for $\sqrt{s} = 500$ GeV and $m_* = 150$ GeV. (a) l^{-*} and (b) ν^*.

Fig. 5 Differential cross sections [in fb] for the single production of excited charged and neutral leptons in e^+e^- annihilation. (a) $\sqrt{s} = 200$ GeV and $m_* = 150$ GeV; (b) $\sqrt{s} = 500$ GeV and $m_* = 300$ GeV.

Fig. 6 Longitudinal and transverse polarisations of the singly produced excited leptons in e^+e^- collisions, as a function of the scattering angle. (a/b) $P_{\|}/P_{\perp}$ at $\sqrt{s} = 200$ GeV and with $m_* = 150$ GeV; (c/d) $P_{\|}/P_{\perp}$ at $\sqrt{s} = 500$ GeV and with $m_* = 300$ GeV.

Fig. 7 Total cross sections [in fb] for the single production of excited charged and neutral leptons in e^+e^- annihilation as a function of the mass. (a) $\sqrt{s} = 200$ GeV and (b) $\sqrt{s} = 500$ GeV.

Fig. 8 Feynman diagrams for single excited lepton production in $e\gamma$ collisions. a) $e\gamma \to e^*$ and b) $e\gamma \to \nu_e^* W$.

Fig. 9 Angular distribution (a) and total cross section (b) for the production of excited neutrinos in association with W bosons in $e\gamma$ collisions with a fixed centre of mass energy of 450 GeV.

Fig. 10 Feynman diagrams for excited charged lepton production in $\gamma\gamma$ collisions. a) pair production and b) single production.

Fig. 11 Total cross sections [in fb] for the pair production of excited charged leptons in $\gamma\gamma$ annihilation as a function of the mass. The full lines are for the usual vector couplings and the dashed lines include the effects of form factors: $f_1 = v^V(1 + s/\Lambda^2)$ and $f_2 = m_*^2/\Lambda^2$ with $\Lambda = 1$ TeV. The center of mass energy has been fixed at $\sqrt{s} = 400$ GeV.

Fig. 12 Angular distributions (a) and total cross sections (b) for the single production of charged excited leptons in $\gamma\gamma$ collisions; the center of mass energy has been fixed at $\sqrt{s} = 400$ GeV. For the total cross sections we also show the effect of a cut $|\cos\theta| < 0.8$ which give the same cross-section for all flavours.

Fig. 13 Feynman diagrams for the production of excited electrons and excited electronic neutrinos in eP collisions.

Fig. 14 Total cross sections for the single production of charged and neutral excited leptons in eP collisions as a function of the mass. (a) $\sqrt{s} = 314$ GeV and (b) $\sqrt{s} = 1.26$ TeV. For the e^*, the contributions of the elastic and inelastic [with $Q^2 > 5$ GeV^2 and $Q^2 < 5$ GeV^2] cross sections are also shown separately.

Fig. 15 The transverse momentum distribution for the single production of excited neutrinos in eP collisions. (a) For $\sqrt{s} = 314$ GeV with $m_* = 100, 150$ and 200 GeV and (b) $\sqrt{s} = 1.26$ TeV with $m_* = 300, 600$ and 900 GeV. The solid curves are for the smallest masses and the dashed curves for the largest ones.

Fig. 16 The transverse momentum distribution for the single production of excited electrons in eP collisions. (a) For $\sqrt{s} = 314$ GeV with $m_* = 100, 150$ and 200 GeV and (b) $\sqrt{s} = 1.26$ TeV with $m_* = 300, 600$ and 900 GeV. The solid curves are for the smallest masses and the dashed curves for the largest ones.

Fig. 17 Longitudinal and transverse polarisations of the singly produced excited leptons in eP collisions, as a function of $\sqrt{Q^2}$. (a) $\sqrt{s} = 314$ GeV, $m_* = 100$ GeV and (b) $\sqrt{s} = 1.26$ TeV, $m_* = 300$ GeV.

m_{ν^*} (GeV)	$\nu^* \to \nu\gamma$	$\nu^* \to \nu Z$	$\nu^* \to eW$
50	55/0	12/25	33/75
75	10/0	18/19	72/81
95	0.25/0	5/4.9	94.75/95.1

Table 1. a

m_{ν^*}(GeV)	$\nu^* \to \nu\gamma$	$\nu^* \to \nu Z$	$\nu^* \to eW$	$\Gamma_{\rm tot}$ (GeV)
100	0	13	87	8.3×10^{-4}
250	0	38	62	8.9×10^{-2}
500	0	39	61	0.81

Table 1. b

m_{e^*}(GeV)	$e^* \to e\gamma$	$e^* \to eZ$	$e^* \to \nu W$	$\Gamma_{\rm tot}$ (GeV)
100	72	1.2	26.8	2.7×10^{-3}
250	31.5	10.5	58	9.6×10^{-2}
500	28.7	11.3	60	0.85

Table 1. c

	e^*	ν_e^*	μ^*, τ^*	ν_μ^*, ν_τ^*
machine	m^* Λ (GeV) (TeV)	m^* Λ (GeV) (TeV)	m^* Λ (GeV) (TeV)	m^* Λ (GeV) (TeV)
LEP100 Present	90 1.12 (t-channel) 50 2.3 (s-channel)	90 0.08 ($\nu^* \to eW$) 50 1.28 ($\nu^* \to eW$)	90 0.45 s-channel 50 1.6 (τ^*) s-channel	– – – – No search for $f = f'$ – – – – No search for $f = f'$
LEP200 $\mathcal{L} = 500 {\rm pb}^{-1}$	180 5.5	150 1.3	150 0.43	150 0.35
e^+e^- $\sqrt{s} = 500$ GeV $\mathcal{L} = 10$ fb^{-1}	450 24.5 400 26.0 300 30.0	450 3.2 400 6.5 300 15.0	450 2.2 400 3.0 300 3.9	450 1.8 400 2.3 300 3.0
$e\gamma$ $\sqrt{s} = 450$GeV	< 450 120	300 37. 350 26.	$\otimes$ $\otimes$	$\otimes$ $\otimes$
$\gamma\gamma$ $\sqrt{s} = 400 GeV$	390 55	$\otimes$	(μ^*) 390 26	$\otimes$
HERA $\sqrt{s} = 314$ GeV $\mathcal{L} = 100 {\rm pb}^{-1}$	160 1.0 100 2.0	150 0.3 80 0.5	$\otimes$ $\otimes$	$\otimes$ $\otimes$
LEP $\oplus$ HLC $\sqrt{s} = 1.26$TeV $\mathcal{L} = 10^3 {\rm pb}^{-1}$	400 4.0 850 1.0	400 2.0 700 1.0	$\otimes$ $\otimes$	$\otimes$ $\otimes$

Table 2.

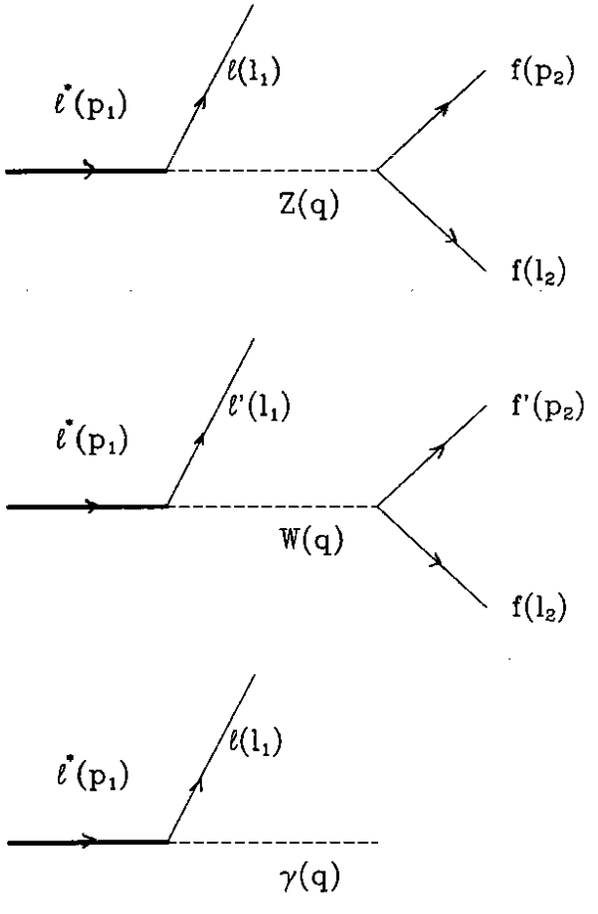
$\ell^*(p_1)$
$\ell(l_1)$
$f(p_2)$
$Z(q)$
$f(l_2)$
$\ell^*(p_1)$
$\ell'(l_1)$
$f'(p_2)$
$W(q)$
$f(l_2)$
$\ell^*(p_1)$
$\ell(l_1)$
$\gamma(q)$

Fig. 1

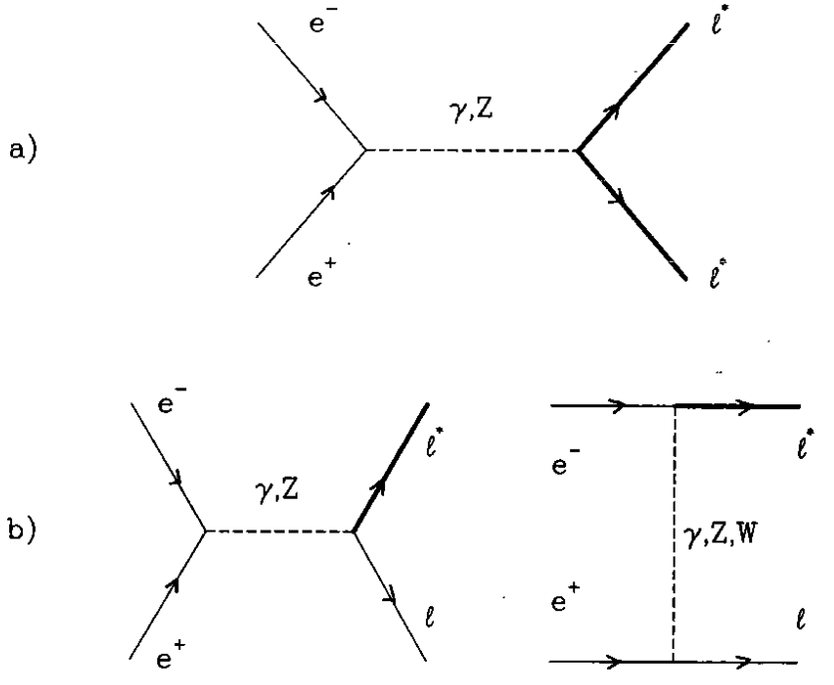
a)
e^-
γ,Z
ℓ^*
e^+
ℓ^*
b)
e^-
γ,Z
ℓ^*
e^+
ℓ
e^-
ℓ^*
γ,Z,W
e^+
ℓ

Fig. 2

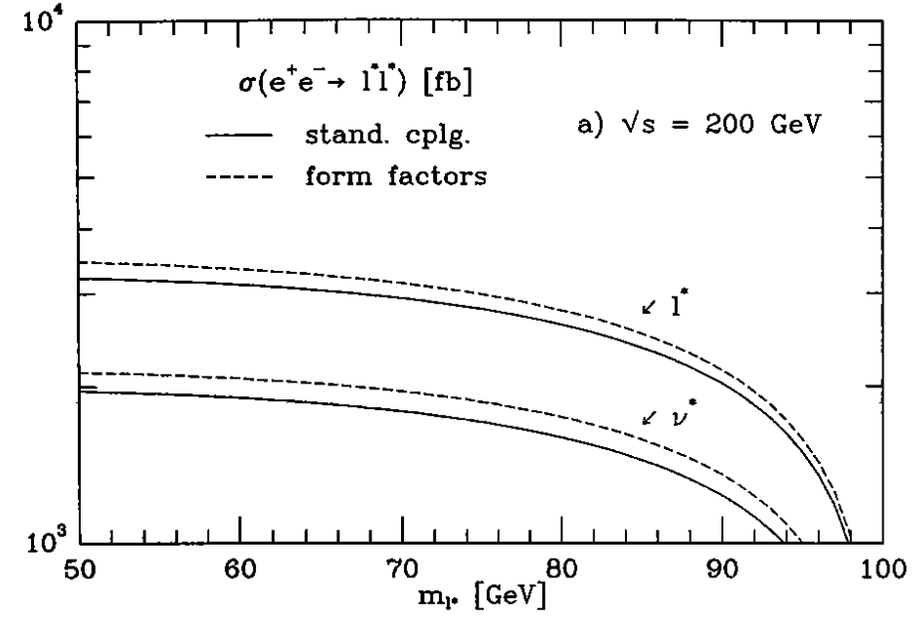
10^4
$\sigma(e^+e^- \to l^*\bar{l}^*)$ [fb]
stand. cplg.
form factors
a) $\sqrt{s}$ = 200 GeV
$\swarrow l^*$
$\swarrow \nu^*$
10^3
50
60
70
80
90
100
m_{l^*} [GeV]

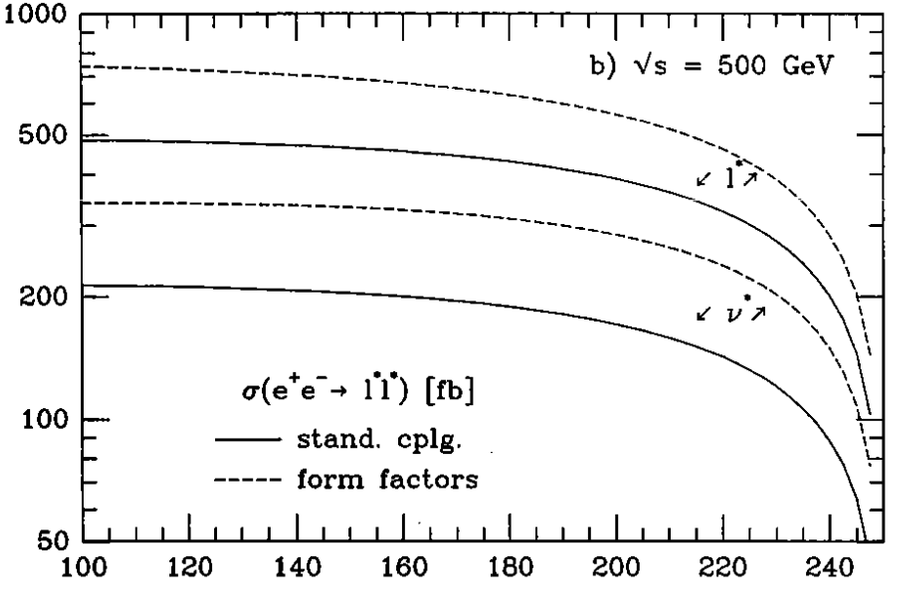
1000
500
200
100
50
b) $\sqrt{s}$ = 500 GeV
$\swarrow l^* \nearrow$
$\swarrow \nu^* \nearrow$
$\sigma(e^+e^- \to l^*\bar{l}^*)$ [fb]
stand. cplg.
form factors
100
120
140
160
180
200
220
240

FIG. 3

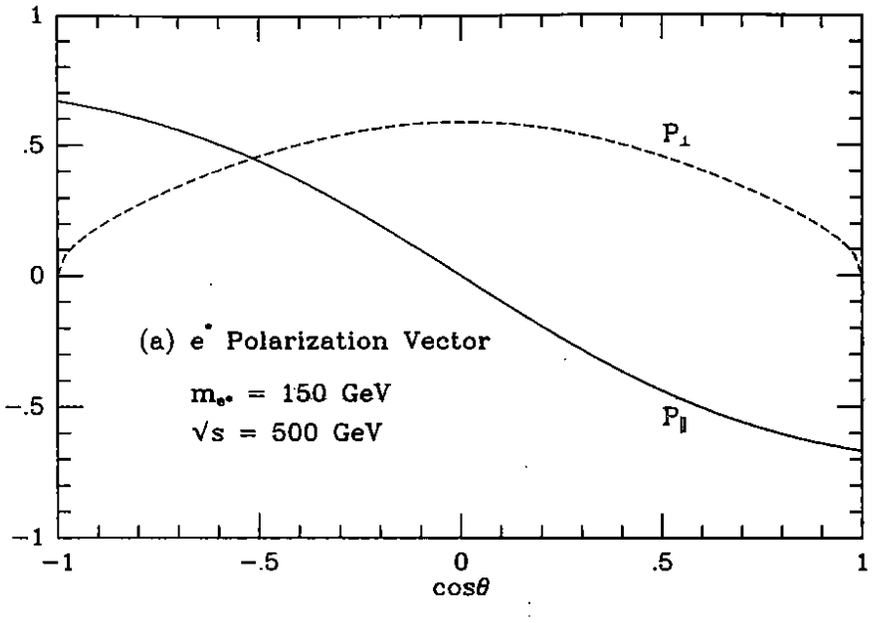
1
.5
0
−.5
−1
$P_\perp$
$P_\parallel$
(a) e^* Polarization Vector
m_{e^*} = 150 GeV
$\sqrt{s}$ = 500 GeV
−1
−.5
0
.5
1
cosθ

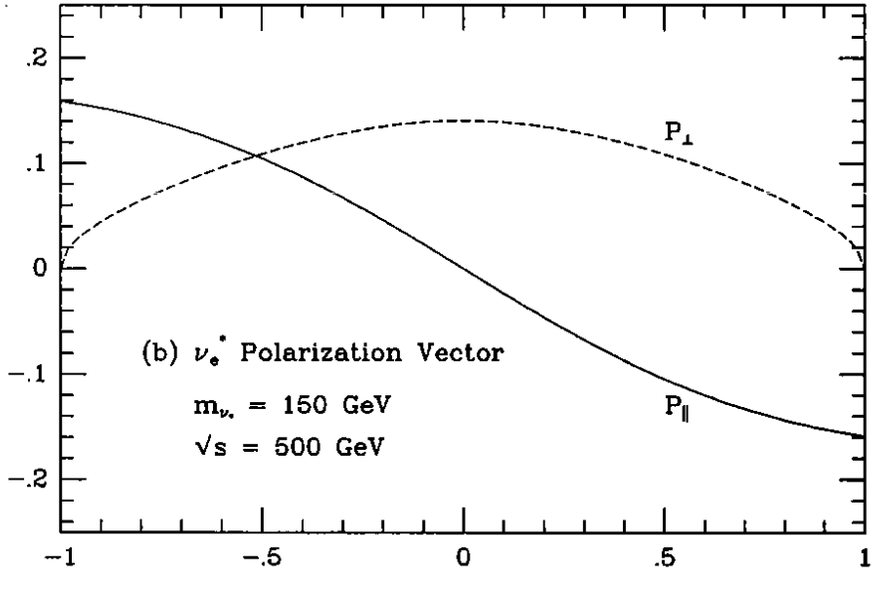
.2
.1
0
−.1
−.2
$P_\perp$
$P_\parallel$
(b) ν_e^* Polarization Vector
m_{ν_e} = 150 GeV
$\sqrt{s}$ = 500 GeV
−1
−.5
0
.5
1

FIG. 4

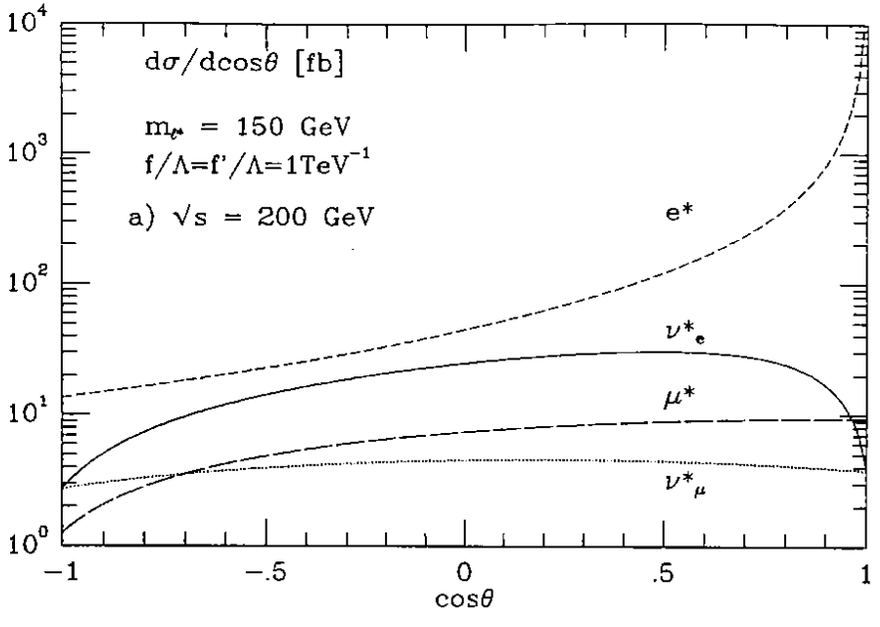
dσ/dcosθ [fb]
m_ℓ* = 150 GeV
f/Λ=f'/Λ=1TeV⁻¹
a) √s = 200 GeV
e*
ν*_e
μ*
ν*_μ
cosθ

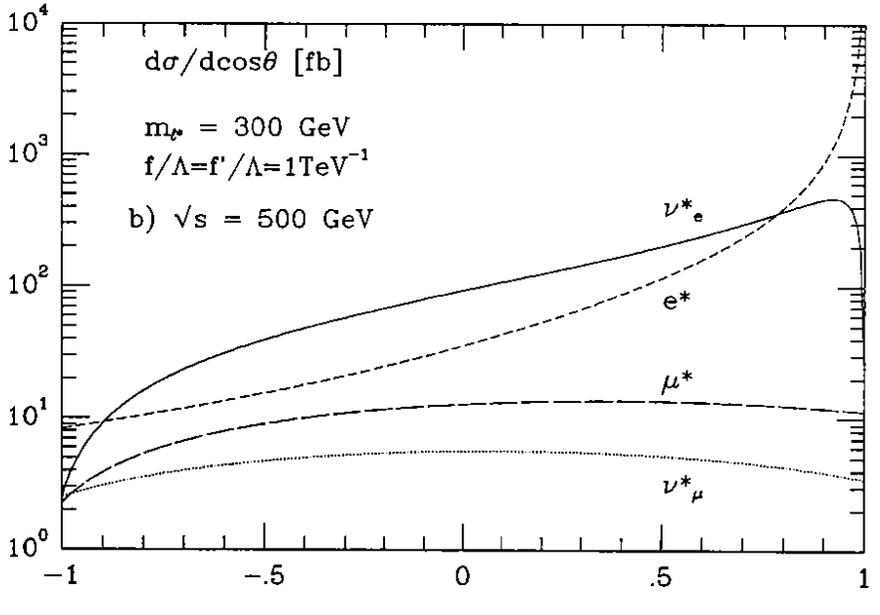
dσ/dcosθ [fb]
m_ℓ* = 300 GeV
f/Λ=f'/Λ=1TeV⁻¹
b) √s = 500 GeV
ν*_e
e*
μ*
ν*_μ

FIG. 5

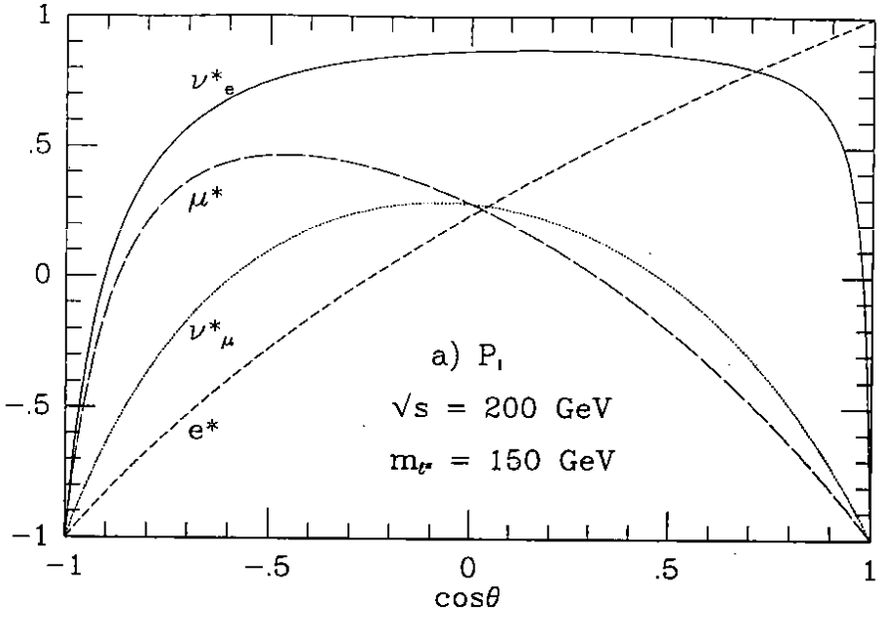
ν*_e
μ*
ν*_μ
e*
a) P_l
√s = 200 GeV
m_ℓ* = 150 GeV
cosθ

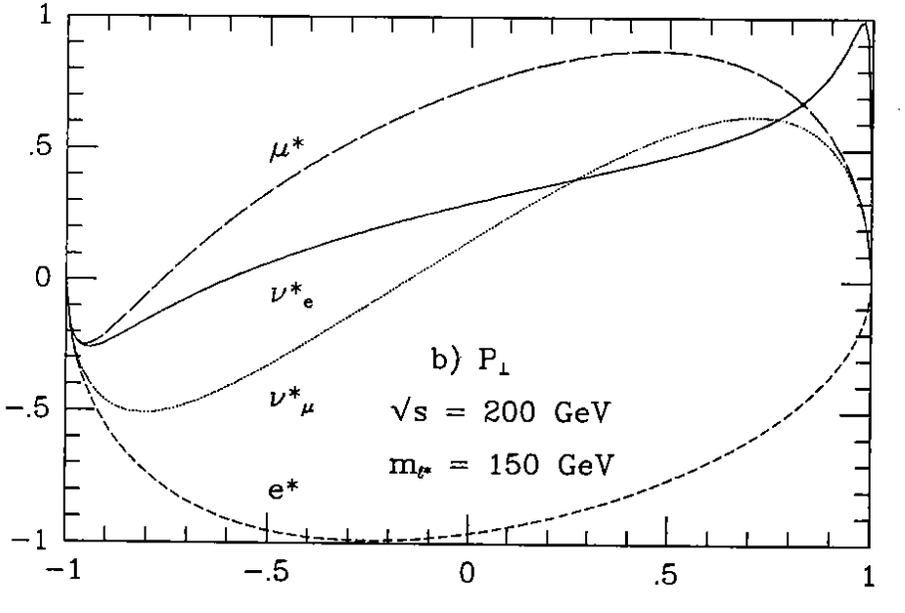
μ*
ν*_e
ν*_μ
e*
b) P_⊥
√s = 200 GeV
m_ℓ* = 150 GeV

FIG. 6

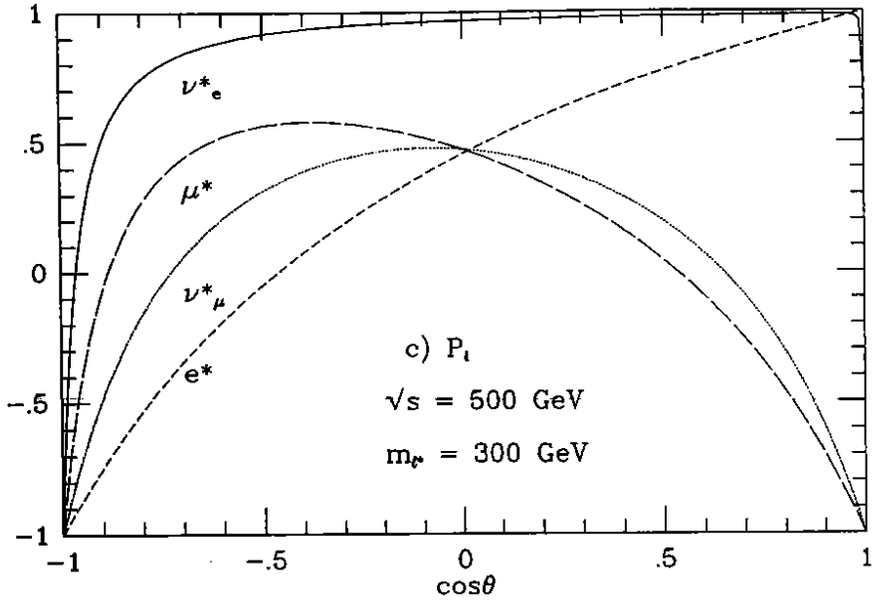

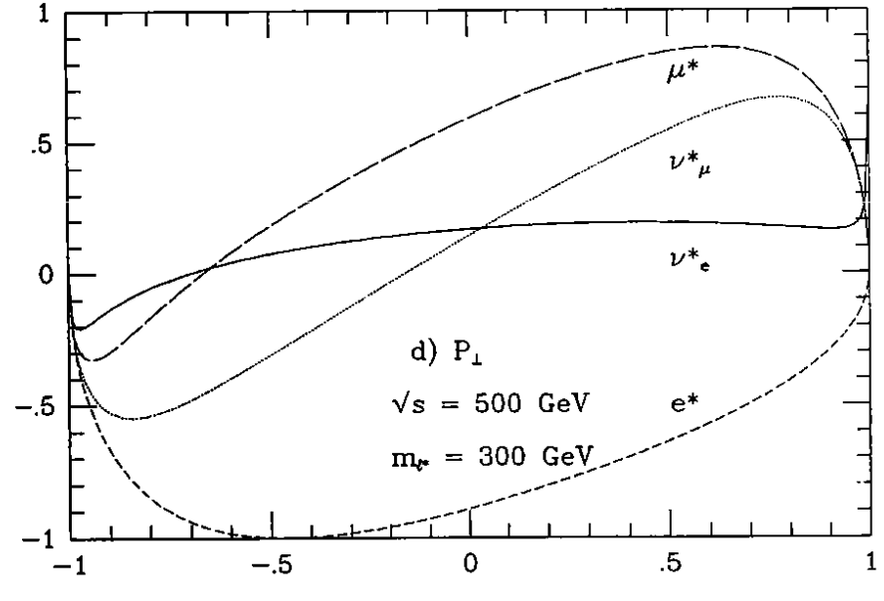

FIG. 6 (cont.)

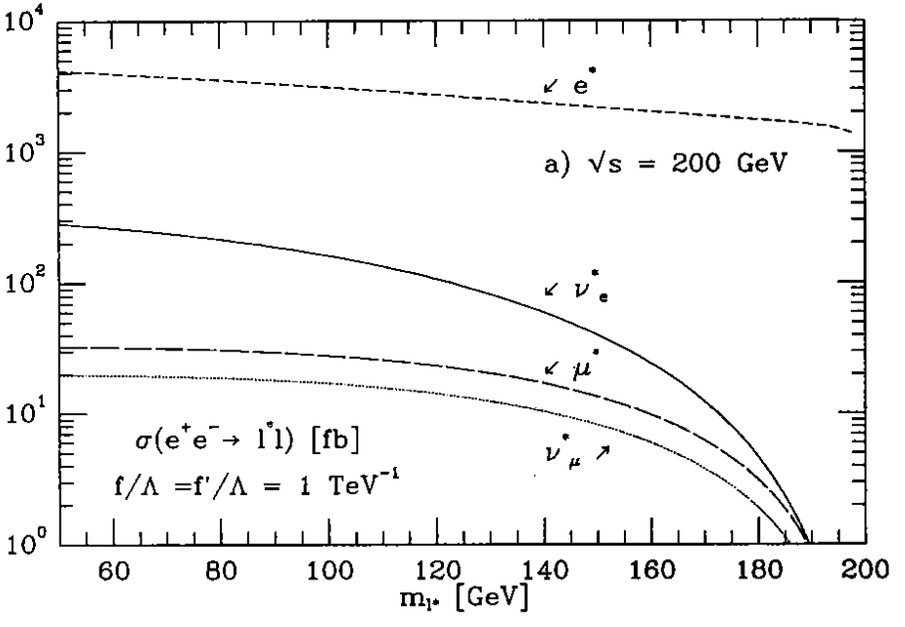

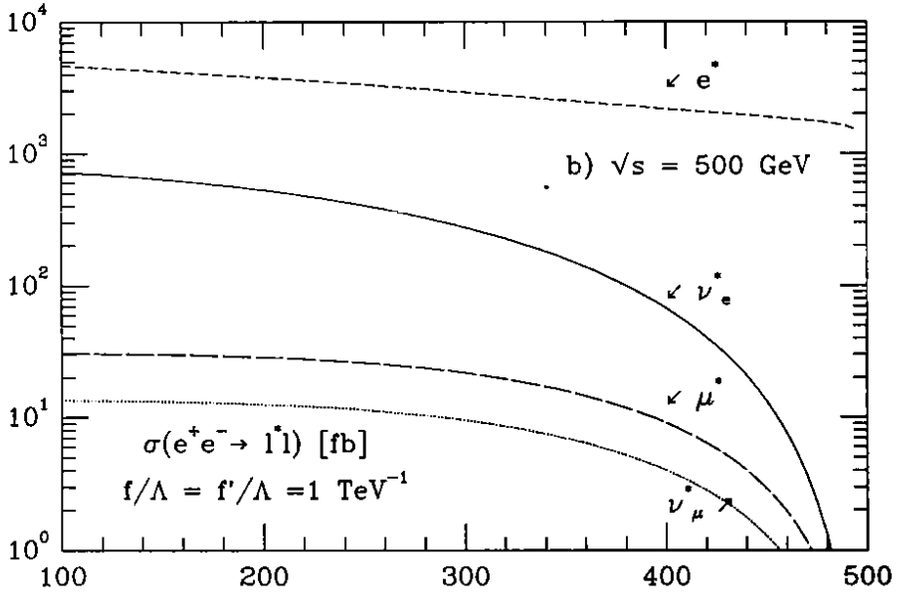

FIG. 7

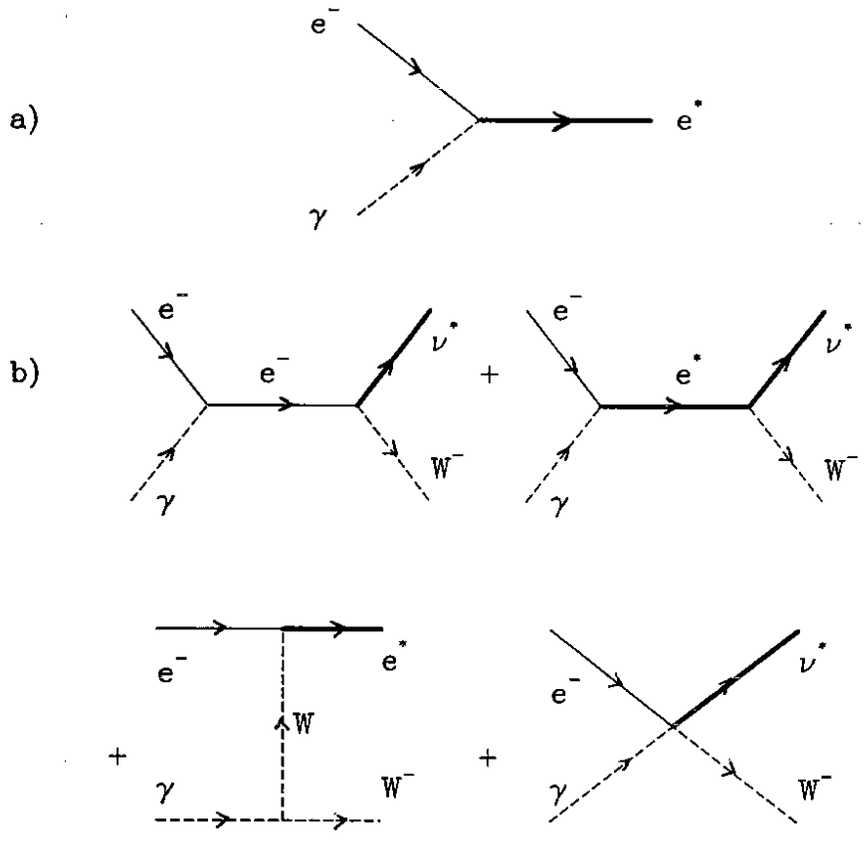
a)
e⁻
γ
e*
b)
e⁻
e⁻
ν*
W⁻
γ
+
e⁻
e*
ν*
W⁻
γ
e⁻
e*
W
γ
W⁻
+
e⁻
ν*
γ
W⁻
+

Fig. 8

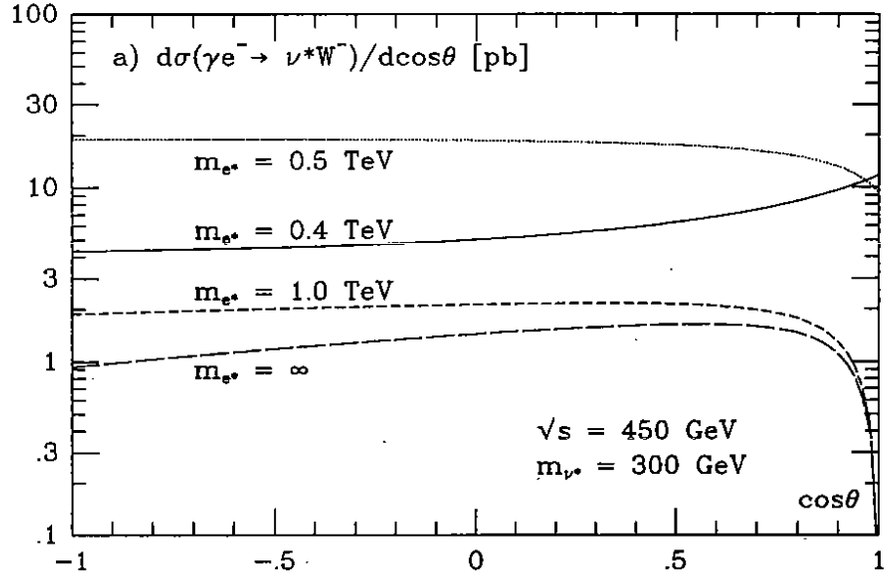
a) dσ(γe⁻→ ν*W⁻)/dcosθ [pb]
m_e* = 0.5 TeV
m_e* = 0.4 TeV
m_e* = 1.0 TeV
m_e* = ∞
√s = 450 GeV
m_ν* = 300 GeV
cosθ
100
30
10
3
1
.3
.1
−1
−.5
0
.5
1

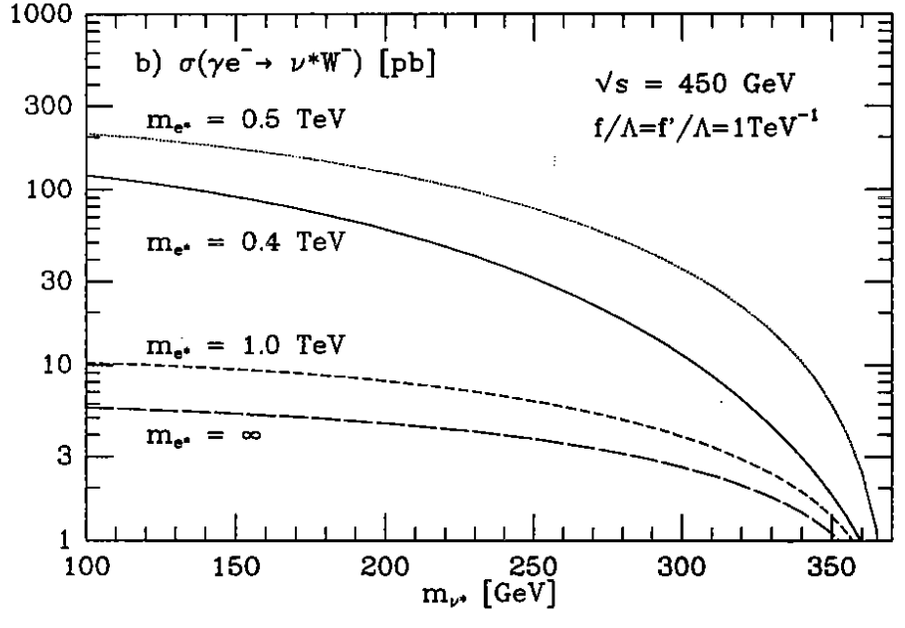
b) σ(γe⁻→ ν*W⁻) [pb]
√s = 450 GeV
f/Λ=f'/Λ=1TeV⁻¹
m_e* = 0.5 TeV
m_e* = 0.4 TeV
m_e* = 1.0 TeV
m_e* = ∞
m_ν* [GeV]
1000
300
100
30
10
3
1
100
150
200
250
300
350

FIG. 9

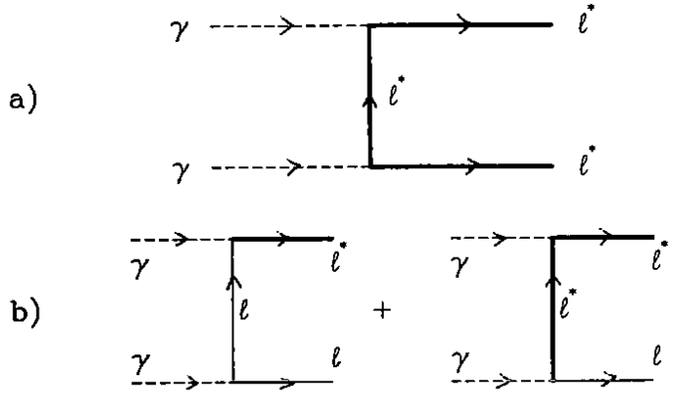

FIG. 10

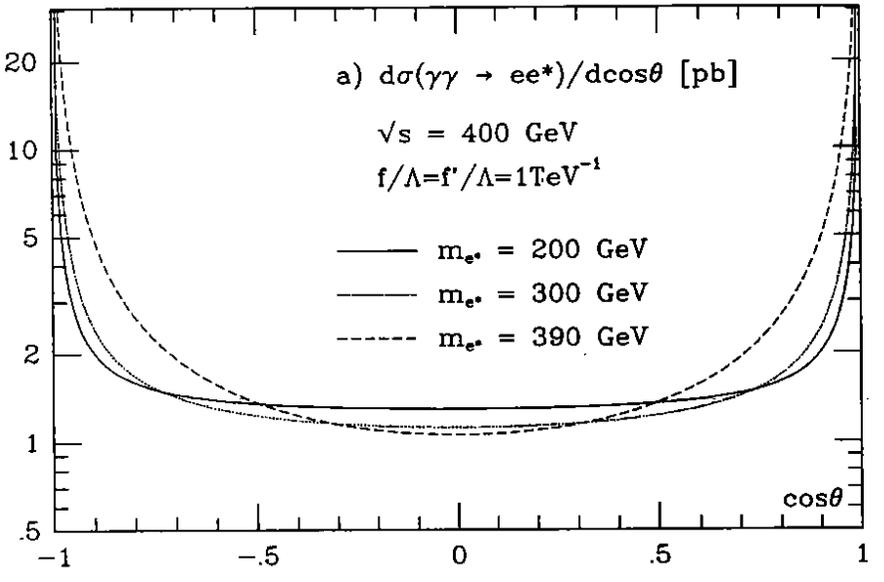

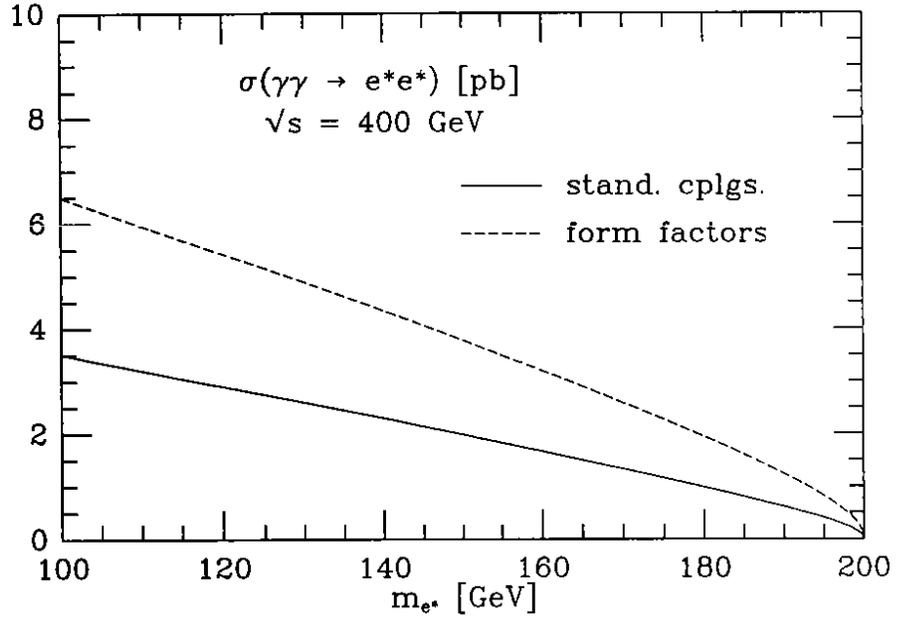

FIG. 11

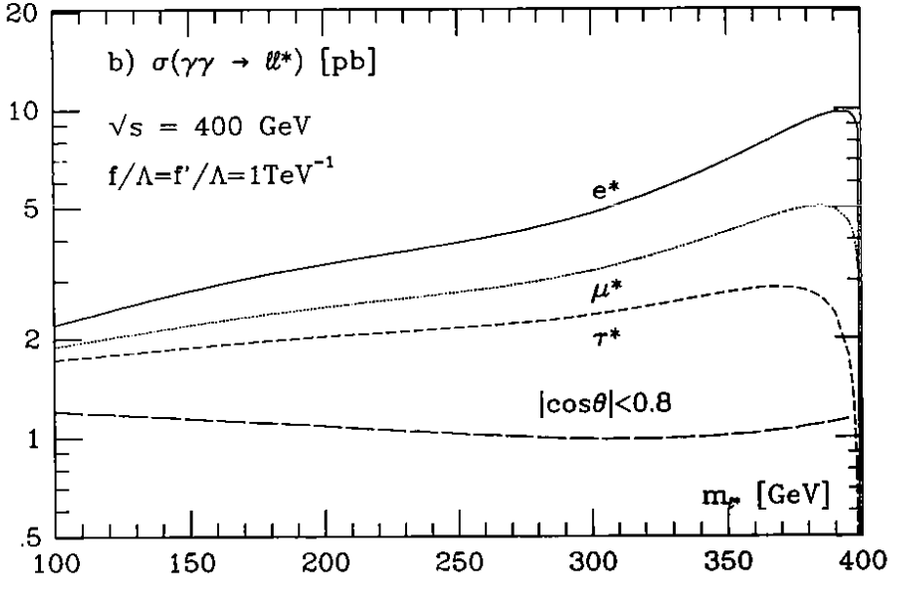

FIG. 12

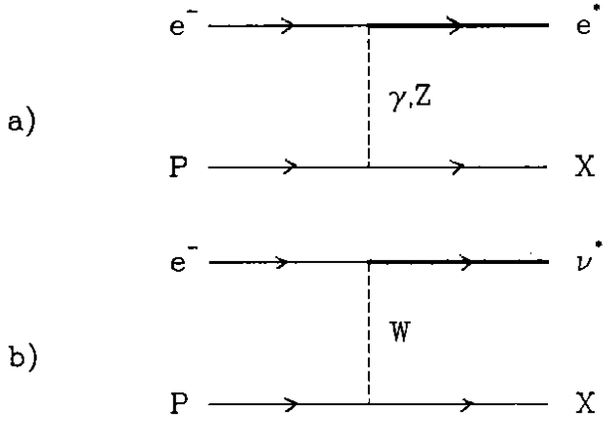
a)
e⁻
e*
γ,Z
P
X
b)
e⁻
ν*
W
P
X

Fig. 13

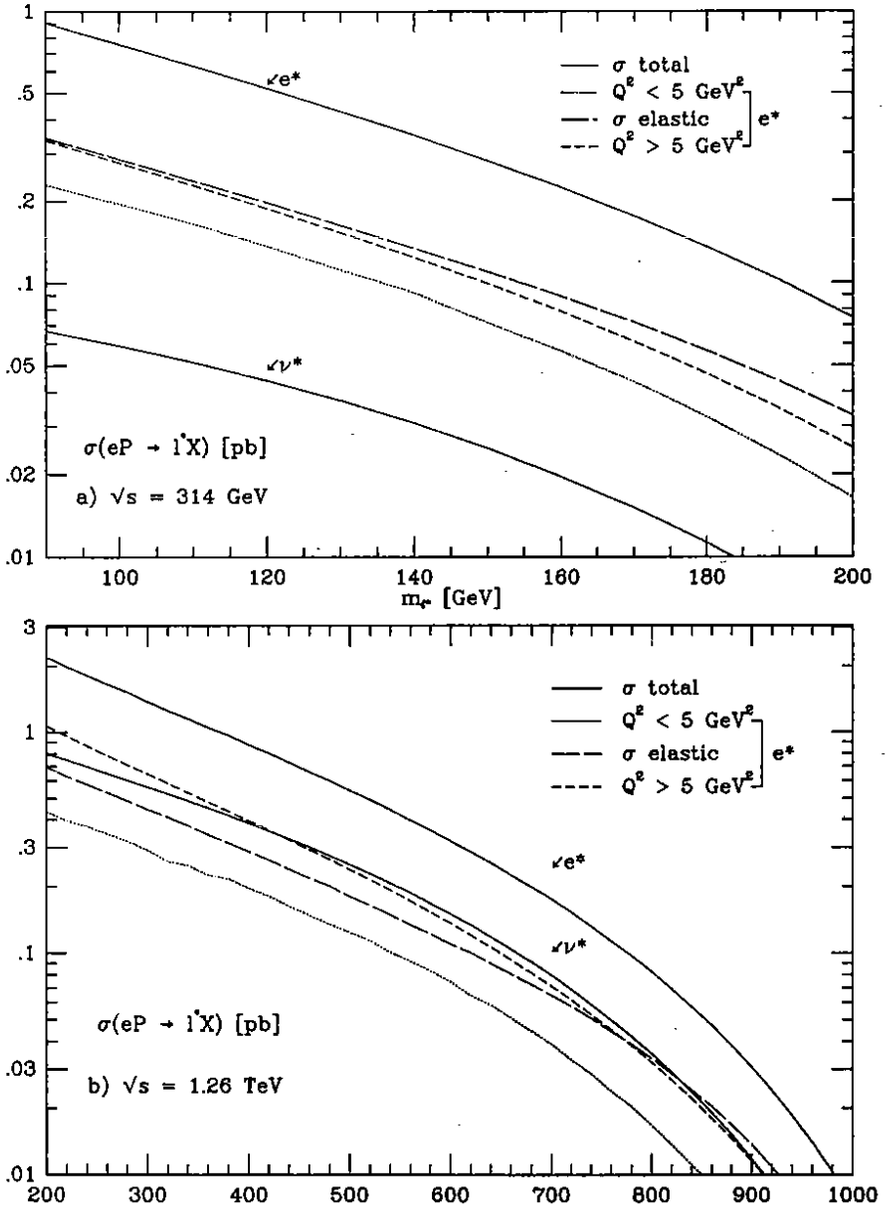
σ total
Q² < 5 GeV²
σ elastic
Q² > 5 GeV²
e*
↙e*
↙ν*
σ(eP → l*X) [pb]
a) √s = 314 GeV
m_e* [GeV]
σ total
Q² < 5 GeV²
σ elastic
Q² > 5 GeV²
e*
↙e*
↙ν*
σ(eP → l*X) [pb]
b) √s = 1.26 TeV

FIG. 14

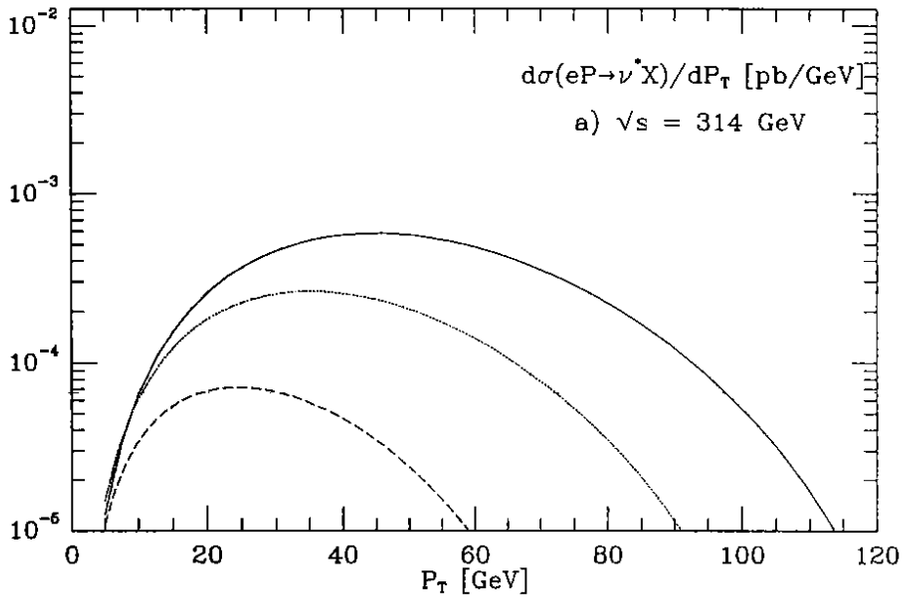
$d\sigma(eP\to\nu^{\bullet}X)/dP_T$ [pb/GeV]
a) $\sqrt{s}$ = 314 GeV
10^{-2}
10^{-3}
10^{-4}
10^{-5}
0
20
40
60
80
100
120
P_T [GeV]

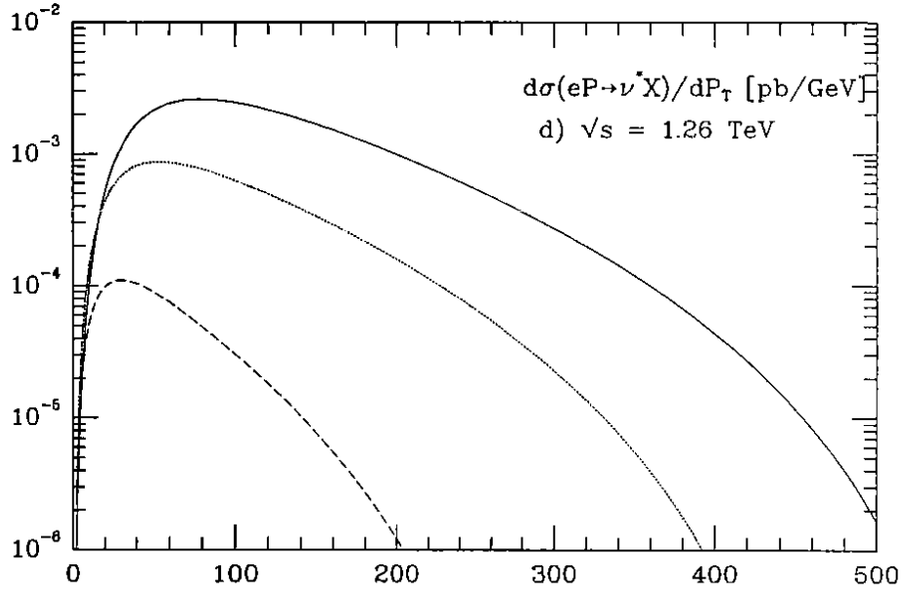
$d\sigma(eP\to\nu^{\bullet}X)/dP_T$ [pb/GeV]
d) $\sqrt{s}$ = 1.26 TeV
10^{-2}
10^{-3}
10^{-4}
10^{-5}
10^{-6}
0
100
200
300
400
500

FIG. 15

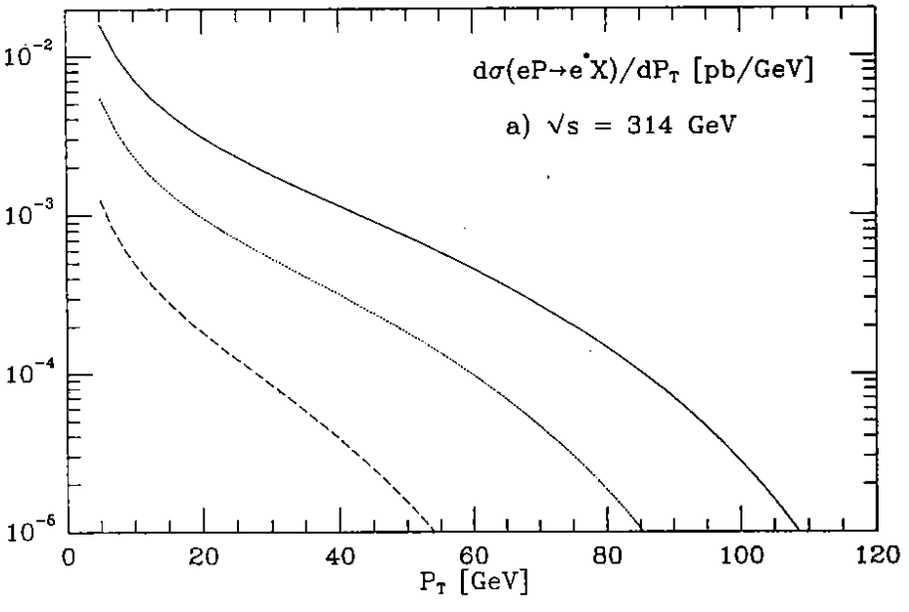
$d\sigma(eP\to e^{\bullet}X)/dP_T$ [pb/GeV]
a) $\sqrt{s}$ = 314 GeV
10^{-2}
10^{-3}
10^{-4}
10^{-5}
0
20
40
60
80
100
120
P_T [GeV]

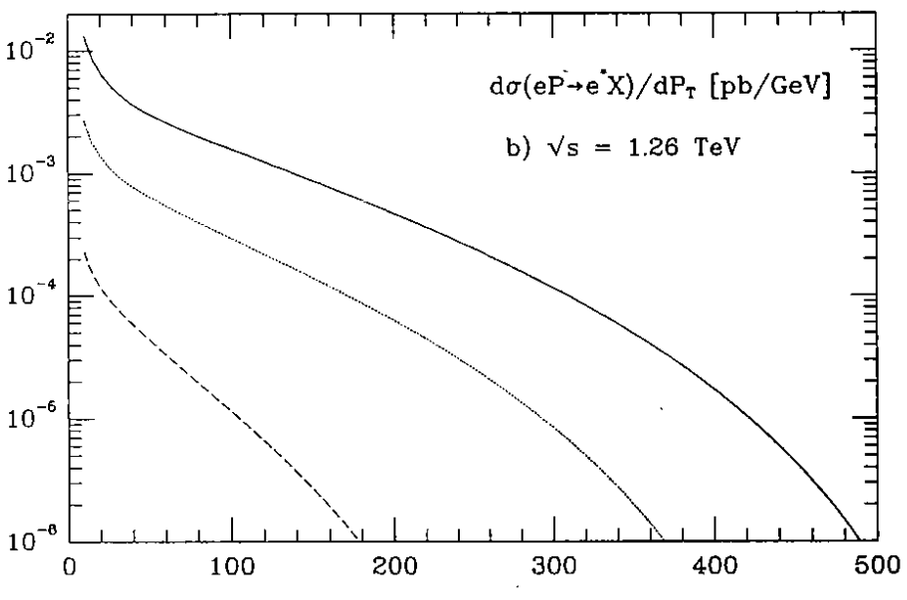
$d\sigma(eP\to e^{\bullet}X)/dP_T$ [pb/GeV]
b) $\sqrt{s}$ = 1.26 TeV
10^{-2}
10^{-3}
10^{-4}
10^{-5}
10^{-6}
0
100
200
300
400
500

FIG. 16

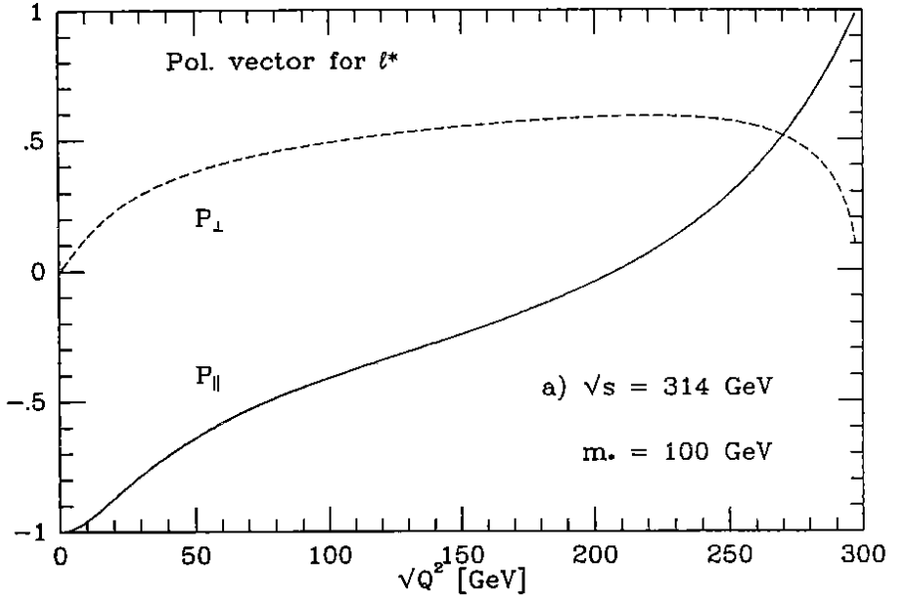
Pol. vector for ℓ*
P⊥
P∥
a) √s = 314 GeV
m* = 100 GeV
√Q² [GeV]
1
.5
0
-.5
-1
0
50
100
150
200
250
300

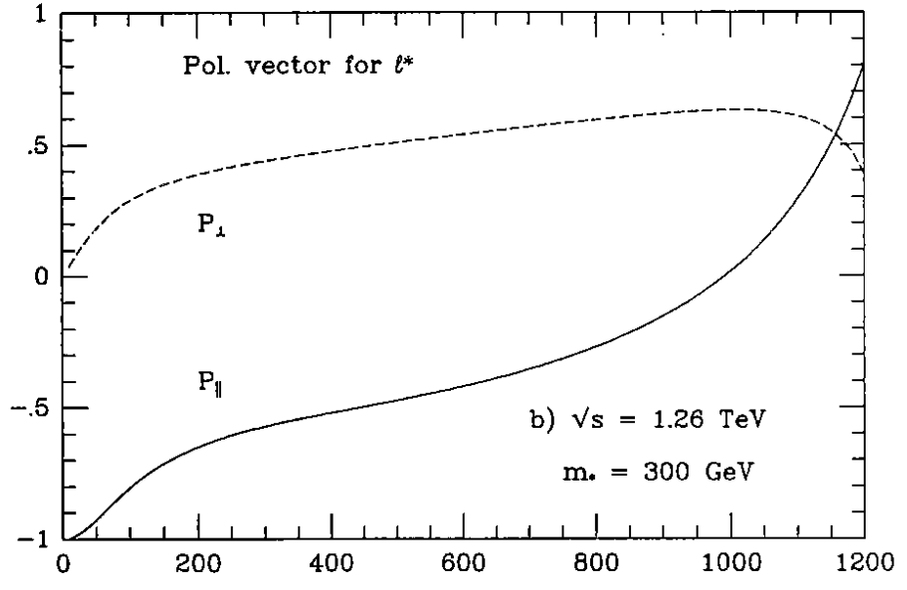
Pol. vector for ℓ*
P⊥
P∥
b) √s = 1.26 TeV
m* = 300 GeV
1
.5
0
-.5
-1
0
200
400
600
800
1000
1200

FIG. 17